Numerical study of a coastal current on a steep slope in presence of a cape: the case of the Promontorio di Portofino.

by

Andrea M. Doglioli[1], Annalisa Griffa[2,3] and Marcello G. Magaldi[1,3]

1. INFM-DIFI, Università di Genova, Genova, Italy
2. Consiglio Nazionale delle Ricerche, ISMAR, La Spezia, Italy
3. RSMAS/MPO, University of Miami, Miami, Florida, USA

Submitted to:

Journal of Geophysical Research - Oceans

Final

September 20, 2004

Abstract

A process study aimed at investigating the winter circulation in the area of the Promontorio of Portofino (North-Western Mediterranean) is presented, motivated by historical current measurements suggesting the presence of an attached recirculating eddy in the lee of the Promontorio (cape). A sensitivity study is first performed in an idealized setting, considering the interaction of a steady incoming current with the cape. Numerical experiments are performed using both 2D (vertically integrated) and 3D versions of the POM model. From the 2D results, the main controlling parameter appears to be the equivalent Reynolds number Re_f, in agreement with previous historical results. In the 3D case, the dependence on the vertical Ekman number Ek_v is investigated at fixed Re_f and a significant intensification of the attached eddy with respect to the 2D solutions is obtained. The main difference between the 2D and 3D dynamics is the presence of a resolved bottom Ekman layer in 3D, introducing a vertical shear in the incoming current, particularly noticeable in the region of the shelf break. This shear is likely to be responsable for a "secondary circulation" (dominated by Coriolis effect), inducing an inshore surface current and asssociated upwelling in the lee of the cape, and causing the observed eddy intensification. Experiments with realistic bathymetry are performed, and the 3D results are found to be in good qualitative agreement with the measurements. The results are expected to be relevant for biological transport, pointing out to a mechanism for eddy intensification connected with surface inshore transport and upwelling.

1 Introduction

The Promontorio of Portofino is a blunt headland with an abrupt, almost square shape (Figure 1), rising from the ocean with very steep slopes. The Promontorio is situated along the Ligurian coast, in the North-Western Mediterranean Sea, in an area of great turistical importance, close to the major port of Genova. Since 1998, the Promontorio and its surroundings have been declared Marine Protected Area, with the intent to preserve the coastal

and marine ecosystem. Many political and social conflicts have arised since then, from the contrast between the high turistical pressure and the need for a suistanable management of natural resources [*Salmona and Verardi* 2001]. In this framework, an understanding of the local circulation and of its impact on transport [e.g. *Doglioli et al.* 2004; *Aliani et al.* 2003] is of great importance in order to correctly manage the maritime and coastal activities of the area.

The Ligurian coastal circulation is part of the general cyclonic circulation of the Mediterranean Sea [e.g. *Castellari et al.* 2000; *Molcard et al.* 2002]. Historical measurements of the coastal current upstream of the Promontory are available in terms of long current meter time series and hydrographic surveys [*Esposito and Manzella* 1982; *Astraldi and Manzella* 1983; *Astraldi and Gasparini* 1986]. They indicate the existence of a northwestward current flowing approximately along isobath and following the narrow shelf. The current appears well organized and consistent, at least during the winter period, with a transport of approximately 0.3 Sv on the shelf. Shorter current meter time series (order of 1-2 months) are available downstream of the cape close to the coast (SIAM database, http://estaxp.santateresa.enea.it/www/siams/prov102.html). Altough they are not contemporaneous, they suggest the presence of an anticyclonic eddy, associated with an eastward countercurrent in the lee of the cape. The eddy appears persistent for a period of the order of a month, at least in the winter period. These measurements, together with the general interest toward the understanding of the circulation in the area, motivate the present investigation. A process study is carried out and the response of the incoming current to the cape is investigated.

The generation of eddies behind capes or islands has been observed in many coastal flows [*Black and Gay* 1987; *Pattiaratchi et al.* 1986; *Signell and Geyer* 1991; *Farmer and Jiang* 2002], and it is known to have significant consequences in terms of dispersion processes [*Chiswell and Roemmich* 1998; *Wang et al.* 1999] and sediment transport [*Pingree* 1978; *Ferentinos and Collins* 1980; *Bastos et al.* 2002, 2003]. Eddy generation is connected to the ubiquitous phenomenon of current separation occuring in flows in presence of obstacles [e.g. *Batchelor* 1967]. Because of the complex non-linear nature of the phenomenon, a quantitative

prediction of eddy characteristics as function of environmental parameters is hard to achieve. Many different mechanisms, characterized by different non-dimensional parameters, play an important role, including bottom friction processes, vertical and horizontal mixing and stratification.

A very large body of literature exists on the phenomenon of coastal current separation and eddy formation behind a cape, in terms of experimental, numerical and theoretical investigations [e.g. *Boyer and Tao* 1987; *Freeland* 1990; *Geyer* 1993; *Denniss et al.* 1995; *Sadoux et al.* 2000]. Many of the previous numerical process studies have focused on eddy formation in shallow water environment, where vertically averaged 2-dimensional dynamics is appropriate [e.g. *Verron et al.* 1991; *Davies et al.* 1995], often considering highly energetic, time-dependent tidal currents and idealized smooth cape structures [*Signell and Geyer* 1991]. Other studies, especially regarding the effects of flows past inslands, concentrate on the limit of very deep water [e.g. *Coutis and Middleton* 2002]. Here, we consider a steady current flowing on a narrow shelf with steep slope interacting with a blunt, rectangular cape. We focus on the case of weak or homogeneous stratification (winter condition) and consider both 2-dimensional (2D) and 3-dimensional (3D) models specifically addressing the question of wether or not 3D dynamics lead to different eddy characteristics. A series of sensitivity experiments is performed considering an idealized topography and varying the environmental parameters in a realistic range. The results are then applied to the realistic topography case and qualitatively compared with the measurement results.

As it is well known, the coastal ocean is one of the most challenging marine environment to understand and to model [e.g. *Haidvogel and Beckmann* 1998]. Results are often significantly sensitive to parameterization choices and parameter values [e.g. *Pérenne et al.* 2001], so that there is a real need for systematic testing and comparisons of numerical model results. In this framework, the present investigation is expected to provide a contribution in two different directions. On the one hand, it will contribute to our understanding of the eddy generation mechanism and of its parameter sensitivity in presence of shelf and steep slope. On the other hand, it will provide indications on the appropriate model configuration and parameter ranges to be used as a basis for future realistic modelling of the specific area or

of other regions with similar characteristics.

The paper is organized as following. In §2 a detailed description of the area of interest and of the available current information are provided. A brief background summary on previous results on eddy formation behind coastal capes is provided in §3, while the general methodology is presented in §4. Results from numerical experiments with idealized bathymetry are discussed in §5, while results with the realistic topography are presented in §6. A summary and some concluding remarks are given in §7.

2 Study Area and Measurements

The study area is located along the eastern coast of Liguria, in Northern Italy (Figure 1), and it is characterized by a narrow continental shelf with a very steep slope, deepening from 50 to 500 m in a few km. Along this coast, the abrupt headland of the Promontorio of Portofino extends into the sea for more than 4 kilometers, with a roughly quadrangular shape. The southern side of the Promontorio is characterized by submerged steep cliffs, while the western and eastern sides descends more gradually. The geomorphological features and the hydrodynamic conditions favour the development of a rich and very diversified environment [*Salmona and Verardi* 2001; *Cattaneo Vietti et al.* 1982]. Therefore the Italian Environment Ministry declared a marine protected area adjacent to the peninsula in June 1998.

The general circulation in the Ligurian Sea is known to be dominated by a well defined cyclonic gyre, with a seasonal cycle related to the seasonal variations of the atmospheric forcing [*Esposito and Manzella* 1982]. In the coastal area, water coming from both western and eastern sides of the Corsica island (Figure 1) join in the so-called Ligurian coastal current, that flows alongshore roughly following the bathymetry [*Astraldi and Gasparini* 1986]. It is by now established that in winter the flow in the Corsica channel increases, while the flow on the western side of Corsica remains steady during the whole year [*Astraldi and Gasparini* 1986; *Buffoni et al.* 1997].

The resulting circulation in the coastal area of interest (Figure 1) is in the general northwestward direction, following the coast, with only short period af reversal, associated with

northely winds [*Astraldi and Manzella* 1983; *Astraldi and Gasparini* 1986]. During normal conditions the forcing mechanism may be summarized as an alongshore density driven component and a wind-induced setup. The temporal variability of the currents is usually dominated by sub-inertial frequencies, with dominant periods of the order of 2-3 days [*Astraldi et al.* 1990] and 15-20 days [*Astraldi and Manzella* 1983], probably associated with direct meteorological forcing and with topographic waves respectively [*Esposito and Manzella* 1982]. Tidal frequencies are characterized by low energy content in this area.

Historical data from current meter time series are available both upward and leeward of the cape (see black squares positions in Figure 1). Data are archived in the SIAM data base (http://estaxp.santateresa.enea.it/www/siams/prov102.html), and they have been kindly made available to us by the Italian National Agency for New Technologies, Energy and Environment (ENEA) and the National Research Council (CNR). The measurements off Sestri Levante, upstream of the Promontorio, cover a total of $\approx$ 10 months, during 1978-1979. They have been previously analyzed and the results are reported in the literature [*Esposito and Manzella* 1982; *Astraldi and Manzella* 1983; *Astraldi and Gasparini* 1986] together with additional data from hydrographical measurements. The measurements were taken on the 100-m isobath at depths of 16, 50 and 95 m. Measurements downstream of the Promontorio have been taken during shorter periods of approximately 2 months in different seasons during 1993 and 1997. They encompass measurements on the 28-m depth isobath off Camogli, just west of the cape, and measurements on the 35-m depth isobath off Bogliasco, approximately 15 km more to the west. The measurements were taken at depths of 10 and 29 m, respectively.

Here we concentrate on results from the winter period, when the currents are stronger and better defined and stratification is weak. Temperature and salinity profiles measured during various cruises on the Eastern Ligurian shelf show that the thermocline generally disappears in February to April, while stratification starts to erode since November-December [*Astraldi and Manzella* 1983; *Astraldi and Gasparini* 1986]. The choice of the winter period facilitate the setting of our process study and the comparison between 2-D an 3-D models.

The selected periods for the measurements are shown in Table 1. From the 10-months

measurement off Sestri Levante, we select the period from 8 February 1979 to 30 April 1979. The shorter data records of Camogli and Bogliasco only partially cover the end and the beginning of the winter respectively: from 18 April 1997 to 31 May 1997 off Camogli, and from 11 December 1992 to 28 February 1993 off Bogliasco. Since the data belong to different years and the seasonal coverage is only partially satisfactory, the results cannot be used for a quantitative comparison and tuning of the model. Rather, they will be used to suggest patterns and order of magnitude of the velocity field and they will help interpreting the sensitivity results narrowing the parameter range.

Standard analyses have been applied to the data. After a preliminary error check, a moving average filter (with window of 24 hours) has been applied to remove the high frequency signal. The progressive vector diagrams for the Sestri Levante, Camogli and Bogliasco measurements are shown in Figure 2. The data have then been projected on a 'natural' coordinate system, defined by the directions along which the standard deviations are extrema and which corresponds to the shear Reynolds stresses vanishing [*Astraldi and Manzella* 1983]. The statistics of the current are presented in Table 1, where (u,v) indicate the mean values and (u',v') the standard deviations of the along and cross components respectively, and θ is the 'natural' rotation angle (measured clockwise with respect to true north).

The results in Figure 2a,b,c indicate that the current off Sestri Levante is northwestward and coherent at all depth, suggesting a significant barotropic component. The alongshore component of the mean flow is well defined, with small variability, and it decreases with depth varying between 37.8 cm/s at 16 m to 18.9 cm/s at 95 m (Table 1). The vertical average velocity appears to be of the same order as the mean at the intermediate depth of 50 m, i.e. $\approx$ 25 cm/s. Nearshore off Camogli (i.e. directly in the lee of the cape), the current is approximately in the opposite, southeastward direction with a mean of 2.3 cm/s in the alongshore component and a more pronounced variability (Table 1). The southeastward direction is persistent during the central measurement period of $\approx$ 25-30 days, while short period reversals can be observed at the beginning and at the end of the time serie (Figure 2d). Nearshore off Bogliasco (about 15 km downstream of the cape), the current is again directed northwestward, as upstream of the cape, and the direction appears well defined during most

of the measurements (Figure 2e). The along velocity component has a mean of 5.3 cm/s (Table 1).

These results provide some interesting suggestions on the pattern of the current in the study area, that will be used in the following process study. The dominant southwestward current at Camogli in the lee of the cape, suggests the existence of a recirculating eddy, with an intensity of the order of $\approx$ 10% of the incoming current. The zonal extension of the eddy appears to be no more than $\approx$ 15 km from the cape, since the downstream current off Bogliasco is northwestward. Finally, the fact that the downstream current direction appears persistent, (over the whole measurement period off Bogliasco and for $\approx$ 1 month off Camogli), suggests that the eddy is attached to the cape, rather than propagating along the shelf [*Signell and Geyer* 1991]. Occasional current inversions off Camogli, where the current is weak, may be due to local atmospheric forcing. This general pattern coincides with what is traditionally known by the Camogli fishermen (personal comunication).

3 Background

The study of current separation and eddy formation behind a cape has a very long history in the literature, going back to the first fluid dynamical investigations on flows past solid bodies [*Batchelor* 1967]. In classical fluid dynamics studies, the main mechanism for separation is provided by lateral friction and the main controlling parameter is the Reynolds number Re. In simple and qualitative terms, the process can be explained as follows. Given a current flowing past a body (the cape), for high enough Re, viscous boundary layers form along the walls, where vorticity tends to be confined. The interior flow, which is irrotational and obeys Bernoulli's equation, accelerates as it aproaches the tip of the cape reaching a maximum velocity at the tip itself. The maximum velocity is associated with a pressure minimum, so that downstream of the tip there is an adverse pressure gradient acting on the interior flow and on the edge of the boundary layer. This adverse pressure gradient subtracts momentum to the boundary layer flow, inducing possible flow reversal. When this happens, the boundary layer detaches and vorticity enters in the interior, forming eddy structures

downstream of the cape.

This mechanism might be applicable also to oceanographical flows, for instance for "dynamically deep" flows around an island [e.g. *Coutis and Middleton* 2002]. In general, though, for coastal flows, the main friction mechanism is usually given by bottom friction, rather than by lateral friction [e.g. *Wolanski et al.* 1984]. Bottom friction is generally higher close to the coast, where the flow is shallower, and it provides a mechanism for vorticity generation and for possible boundary layer confinement near the coast. The main parameter, in this case, is an equivalent Reynolds number Re_f [*Pingree* 1978], given by the ratio between advection and bottom friction terms (exact definitions of the non-dimensional parameters are given in §4.4 using specific flow parameter). Re_f has been shown to effectively control the flow, at least in first approximation, in a number of numerical and experimental investigations of shallow flows past islands or capes [*Pattiaratchi et al.* 1986; *Signell and Geyer* 1991; *Davies et al.* 1995]. For very small Re_f, when friction dominates, the flow tends to follow the cape without separating. At increasing Re_f, laminar separation occurs and an "attached" stationary eddy forms in the lee of the cape. For higher Re_f, the eddy detaches and propagates downstream, leading to an "eddy-shedding" unstable regime. Finally, at very high Re_f, a fully developed turbulent wake develops.

While Re_f seems to be the main controlling factor, also other parameters appear to play a role in eddy formation in coastal flows. For realistic velocities and space scales of the order of kms, background rotation plays an important role in the dynamics. The impact of rotation on flow separation has been studied [*Merkine and Solan* 1979; *Davies et al.* 1995] as function of the Rossby number Ro and of the Ekman number Ek_v, indicating respectively the ratio of advection and viscosity with respect to the Coriolis effect. In presence of stratification, also the Burger number Sb, representing the ratio between the Rossby radius of deformation and the typical length scale of the flow, has to be considered [e.g. *Boyer and Tao* 1987]. Finally, we point out that, for differential background rotation, as in the case of β-plane, flow separation and eddy formation are also influenced by the direction of the incoming current with respect to the direction of propagation of the free Rossby waves [e.g. *Merkine* 1980; *Tansley and Marshall* 2001]. For eastaward flows, β tends to inhibit the separation and

the formation of downstream attached eddies, while it does not have a significant influence in the case of westard flows. Analogous results hold for topographic Rossby waves induced for instance by shelf topography [*Brooks* 1990; *Freeland* 1990; *Yankovski and Chapman* 1997]. When the incoming current opposes to wave propagation, the flow structure is strongly altered, favoring the formation of offshore directed flows and jets.

Concerning our application to the Promontorio of Portofino, we expect that planetary β will not play a role, given the small scales of the domain, while the topographic effects can be relevant given the steep slope. Topographic waves, though, have the same westward direction as the main incoming current, so that they are not expected to significantly alter the flow. In the process study presented in §5 and §6, realistic ranges of the various parameters Re_f, Ro, Ek_v, Sb are considered, and sensitivity tests are performed, in order to investigate the role of the various physical mechanisms.

4 Method

In this work, a process study is performed, motivated by the data results, to understand the basic processes of eddy formation in the case of steep slope and narrow shelf. At this end, a numerical model with simplified geometry and bathymetry is considered first and a sensivity study is performed.

4.1 Idealized Physical System

The real system (Figure 1) is idealized as shown in Figure 3a. To ensure that the main flow direction is perpendicular to the open boundaries of the numerical domain, the whole domain has been rotated by 27 degrees anticlockwise with respect to true North. The coastline is simplified to obtain a rectangular headland, whith approximatively the same dimensions as the Promontorio of Portofino: $a = 6$ km defines the length (or alongshore extent) and $b = 5$ km defines the width (or cross-shore extent). The bathymetry cross-shore profile is idealized using an exponential profile:

$$H(y) = H_{min} \mathrm{e}^{2\lambda(Y_o - y)} \ , \tag{1}$$

where H_{min} is the minimum depth and Y_o is the minimum depth isobath ordinate. The parameter values were chosen to fit the real topography up to 500-m depth (see Figure 3b, where solid line represents the exponential function and dotted lines represent several real depth cross-shore profiles). The resulting values are: $H_{min} = 20$ m $Y_o = 46.5$ km and $\lambda = 0.0002$ m^{-1}. Beginning from the 500-m isobath, the real topography is drastically simplified considering flat bottom.

A steady current entering the domain from the eastern boundary is prescribed, and its interaction with the cape is studied.

4.2 Model Equations

The equations governing the flow are the hydrostatic Boussinesq primitive equations:

$$\nabla\cdot \mathbf{u} + \frac{\partial w}{\partial z} = 0 \ , \tag{2}$$

$$\frac{\mathrm{d}\mathbf{u}}{\mathrm{d}t} + \mathbf{f}\times\mathbf{u} + g\nabla\eta + \nabla p = \frac{\partial}{\partial z}\left(K_M\frac{\partial \mathbf{u}}{\partial z}\right) + \nabla\cdot(A_M\nabla\mathbf{u}) \ , \tag{3}$$

$$\frac{\partial p}{\partial z} = -g\frac{\rho}{\rho_o} \tag{4}$$

supplemented with conservation equations for temperature and salt concentration, and an equation of state linking density to temperature and salinity.

Here, $\mathbf{u} \equiv (u, v)$ is the horizontal velocity vector; w, the vertical velocity; $\mathbf{f}$, the vertical Coriolis vector; g, the gravitational acceleration; η, the surface displacement; ρ_o, a constant reference density; ρ, the departure of the total density from ρ_o; p, the baroclinic pressure divided by ρ_o; K_M and A_M are the vertical and horizontal eddy viscosity coefficients. Finally, ∇ stands for the two-dimensional horizontal gradient operator and $\frac{\mathrm{d}}{\mathrm{d}t}$ is the material derivative following the particel: $\frac{\mathrm{d}}{\mathrm{d}t} = \frac{\partial}{\partial t} + \mathbf{u}\cdot\nabla + w\frac{\partial}{\partial z}$.

In order to solve numerically the equations, the Princeton Ocean Model [POM, version pom98; *Mellor* 1998] has been used. It is a sigma coordinate model in that the basic equations have been cast [*Blumberg and Mellor* 1987] in a bottom following system based on the transformation

$$x^* = x, \ \ y^* = y, \ \ \sigma = \frac{z-\eta}{H+\eta}, \ \ t = t^* \ ,$$

where x, y, z are the conventional cartesian coordinates and $H(x, y)$ is the bottom topography. The sigma coordinate system is a useful attribute in dealing with significant topographical variability.

The vertical boundary conditions for equation (2) is

$$\omega(x, y, 0) = \omega(x, y, -1) = 0 \ , \tag{5}$$

where $\omega(x, y, \sigma)$ is the velocity component normal to sigma surfaces [*Mellor* 1998].

In this study, the wind stress was neglected, while bottom ($\sigma = -1$) boundary condition for equation (3) is

$$\frac{K_M}{H + \eta} \left(\frac{\partial \mathbf{u}}{\partial \sigma} \right) = C_D |\mathbf{u}| \mathbf{u} \ ,$$

where C_D is the bottom friction coefficient [*Mellor* 1998].

The subgrid scale turbulent processes are parameterized in analogy to molecular diffusion [*Blumberg and Mellor* 1987]. In our numerical experiments, horizontal eddy viscosity has been either set constant or calculated following Smagorinsky [*Smagorinsky* 1963; *Mellor* 1998]:

$$A_M = C \Delta x \Delta y \left[\left(\frac{\partial u}{\partial x} \right)^2 + \frac{1}{2} \left(\frac{\partial v}{\partial x} + \frac{\partial u}{\partial y} \right)^2 + \left(\frac{\partial v}{\partial y} \right)^2 \right]^{\frac{1}{2}} \tag{6}$$

while vertical eddy viscosity K_M is set constant in all the runs.

POM adoptes the mode splitting technique [*Blumberg and Mellor* 1987], that permits the calculation of the free surface elevation by solving the volume transport (external mode) separately from the vertical velocity shear and thermodynamics (internal mode). The external mode equations are obtained by integrating the equations (2) and (3) from $\sigma = 0$ to $\sigma = -1$ and using the boundary conditions (5). In our bidimensional experiments the POM external mode was executed by itself, then the so-called dispersion term and the buoyancy term are neglected [*Mellor* 1998]. A quadratic formulation based on depth-averaged velocity was adopted for the bottom friction term: $C_D |\mathbf{U}| \mathbf{U}$, where $\mathbf{U} \equiv (U, V)$ is the depth-average velocity.

4.3 Numerical Setup

The integration domain (see Figure 3a) is 100.5 km long (in the alongshore direction x) and 48.4 km wide (in the cross-shore direction y) and is discretized by a rectangular grid with 202 by 81 points, respectively. The horizontal resolution is $\Delta x = 500$ m in the alongshore direction and varies linearly in the cross-shore direction between $\Delta y = 200$ m (nearshore) and $\Delta y = 1000$ m (offshore). The vertical resolution is discretized by 31 sigma layers. The criterion $\left|\frac{\sigma}{H}\frac{\partial_y H}{\partial \sigma}\right| < 1$ [*Mellor et al.* 1994, 1998] was respected and a refined σ grid near the bottom was adopted and tested.

The domain has one close boundary (the "northern" one), where the no slip condition is assumed, and three open boundaries. At the "eastern" (incoming) open boundary, the upstream inflow is specified using the Flather condition [*Flather* 1976] on the alongshore component of the depth-averaged velocity:

$$U = U_e + \sqrt{gH}(\eta - EL_e) \ , \tag{7}$$

where $U_e = U_e(y)$ is a prescribed cross-shore profile of the alongshore component of the depth-averaged velocity and $EL_e = EL_e(y)$ is the corresponding cross-shore profile of the elevation, computed using the geostrophic approximation. For the depth-dependent velocity, Orlanski radiation conditions [*Orlanski* 1976] are used in order to allow internal waves to radiate out of the domain. Radiation boundary conditions are also used at the "western" (outcoming) boundary to radiate both depth-dependent and barotropic velocity. For temperature T (and analogously for salinity S) at both the "eastern" and "western" boundaries the upstream advection condition [*Mellor* 1998] was used:

$$\frac{\partial T}{\partial t} + u_{bound}\frac{\partial T}{\partial x} = 0 \ ,$$

where $u_{bound} = u(x_{bound}, y, z, t)$ is the alongshore component of the velocity at the boundary. Finally, at the "southern" boundary, since we considere negligible the interaction with the open sea, a free sleep wall was posed. The domain size has been chosen large enough to ensure that the boundary conditions do not interfere with the flow variations caused by the headland.

This setup has been tested following the numerical experiments by *Chapman* [1985]; *Palma and Matano* [1998, 2000]. Furthermore, several tests on the outcoming boundary conditions were performed changing domain size: the internal values calculated by the model on a elongated domain were compared with the boundary values obtained at the western boundary of the standard domain, obtaing a very good agreement. Here it is important to stress that, since the governing boundary condition is posed on the depth-average velocity, the same basic setup can be mantained for both bi- and three-dimensional simulations.

The fluid is rotating and the Coriolis parameter is fixed to $f = 1.03 \times 10^{-4}$ s^{-1}, that is the appropriate value for the latitude of Promontorio di Portofino. The external and internal time steps are set at $\Delta te = 2$ s and $\Delta ti = 60$ s, respectively, so as to satisfy the Courant-Friedrichs-Lewy criterion for numerical stability in both external and internal mode.

Several kinds of initial conditions have been tested, obtaining good results with the in motion condition of undisturbed geostrophic flow with intensity $\mathbf{U}(x, y, t = 0) = U_e$.

4.4 Idealized Bathymetry Experiments and Non-dimensional Parameters

Sensitivity experiments with the idealized topography (Figure 3) have been performed and characterized in terms of non-dimensional parameters. Five different parameters, commonly used in the literature and already introduced in §3, have been considered:

$$\begin{aligned} Re &= \frac{U_o a}{A_M}\,, \text{the Reynolds number ;} \\ Re_f &= \frac{H_o}{C_D a}\,, \text{the equivalent Reynolds number ;} \\ Ro &= \frac{U_o}{fa}\,, \text{the Rossby number ;} \\ Ek_v &= \frac{K_M}{fH_o^2}\,, \text{the vertical Ekman number ;} \\ Sb &= g\frac{\Delta\rho}{\rho}\frac{H_o}{f^2a^2}\,, \text{the Burger number ;} \end{aligned} \tag{8}$$

where U_o is a typical scale for the depth-averaged velocity of the incoming current, H_o is a typical depth scale and $\frac{\Delta\rho}{\rho}$ is the typical density gradient of stratification. Preliminary

investigations, performed varying the bathymetry, suggest that a representative value of depth is given by the bathymetry value offshore at a distance equal to the offset of the cape (see Figure 3a). This correspond to $H_o = 250$ m. In addition to the parameters (8), also the geometrical parameters are expected to play a role, i.e. the ratio between length and width of the cape a/b and the ratios between cape dimensions and reference depth, a/H_o, b/H_o. These parameters are held fixed in all the following experiments and they correspond to $a = 5$ km, $b = 6$ km.

Various sets of experiments have been performed varying the parameters (8), as summarized in Table 2. Our first benchmark experiments, 'C_D2D', are obtained with the 2D model varying Re_f while maintaining constant Ro and Re, in keeping with previous results [*Signell and Geyer* 1991; *Davies et al.* 1995] showing that Re_f is the main controlling parameter. Re_f is varied by varying the bottom friction coefficient C_D in the range $10^{-3} \leq C_D \leq 5 \times 10^{-4}$, being $C_D = 2.5 \times 10^{-3}$ a value commonly used in coastal models [*Signell and Geyer* 1991]. The incoming current U_o and the horizontal viscosity A_M, controlling the Rossby and Reynolds numbers (8) respectively, are held fixed for all the experiments. More precisely, the cross-shore profile of the alongshore component of depth-averaged velocity in equation (7) is set to $U_e = 0.25$ m/s. The U_e value is based on the measurements off Sestri Levante (Table 1), as representative of the depth-average winter velocity. A constant value of horizontal eddy viscosity A_M is used, $A_M = 1$ m^2/s [*Signell and Geyer* 1991]. Preliminary investigations considering the Smagorinsky parametrization (6) with $C = 0.1$ show very similar results. This is not surprising given that the resulting Smagorinsky viscosity has values of the same order. Also, in these experiments the dominant friction mechanism is given by bottom friction, as indicated by $Re >> Re_f$, so that the sensitivity to A_M is weak.

The dependence on the Rossby number for the 2D case is investigated with the 'U_o2D' experiments (Table 2), where the incoming current is varied while keeping the other parameters constant. The bottom friction coefficient is set to $C_D = 0.0025$ while A_M is assigned as in 'C_D2D'. Notice that for these experiments, since U_o varies, also Re varies (Table 2). The dependence on the incoming current is studied considering different intensities and shapes of the inflow boundary current. In particular, we consider three cases with constant inflow,

$U_e(y) = U_e = 0.067, 0.25, 0.50$ m/s, i.e. the mimimum, medium and maximum values of current intensity measured off Sestri Levante. The transport on the shelf and on the slope due to these inflow current intensities is $T_e = 0.08, 0.29, 0.59$ Sv, respectively. Furthermore, a Gaussian cross-shore profile for $U_e(y)$ is also considered, [as in *Yankovski and Chapman* 1995, 1996, 1997], centered on the 100-m isobath and characterized by a realistic alongshore transport on the slope and the shelf of about 0.3 Sv. Various values of s.d. for the Gaussian have been considered, corresponding to different jet widths. Analogous experiments have also been performed in 3D, and they are indicated as '$U_o 3D$' (Table 2).

Other 3D experiments, '$K_M 3D$' (Table 2), investigate the dependence on the vertical Ekman number at constant Ro, Re and Re_f. In this case, the vertical eddy viscosity is varied in the range $10^{-1} \leq K_M \leq 10^{-4}$ m^2/s [e.g *Pedlosky* 1987], while a constant inflow is considered, $U_e = 0.25$ m/s, bottom friction coefficient is $C_D = 0.0025$ and A_M is calculated by Smagorinsky equation (6) with $C = 0.1$. Regarding stratification, in all the 3D runs the salinity is assumed constant at the open boundaries and as initial conditions, $S(x_{bound}, y, z) = S(x, y, z, t = 0) = 38$ psu. For potential temperature, instead, both a constant vertical profile $T(x_{bound}, y, z) = T(x, y, z, t = 0) = 13.5\,^o$C and a linearly varing profile between $14\,^o$C (surface) and $13\,^o$C (bottom) has been considered, in keeping with historical winter measurements [*Astraldi and Manzella* 1983; *Astraldi and Gasparini* 1986]. The resulting Burger number for the runs with weak stratification is $Sb = 6.4$.

The time convergence of the experiment solutions has been assessed considering the behaviour of the total kinetic energy (KE) integrated over the domain. For stationary attached eddies, KE converges to a constant value, while for eddy-shedding time dependent solutions KE tends to an oscillatory function with well defined limiting values. A scaling analysis of the equations of motion suggests that the relevant dimensional adjustment time for cases in which the flow is dominated by bottom friction (as in most of our experiments) is $\hat{\tau} = \frac{H_o}{C_D U_o}$ [*Davies et al.* 1995]. Considering the associated dimensionless time $\tau = t/\hat{\tau}$, in most experiments full adjustment is observed to occurr within $\tau = 2$, while typical duration of the numerical runs is $3 \leq \tau \leq 10$.

5 Results for the Idealized Bathymetry Experiments

Before going into the details of the results, we briefly discuss how to characterize the solutions, both quantitatively and qualitatively. The qualitative description is based on horizontal maps of depth-averaged velocity and depth-averaged vertical component of vorticity. A typical example of velocity map is shown in Figure 4: the inflow current separates at the headland and an anticyclonic eddy appears in the lee. It is also possible to observe a local minimum in the pressure field, as suggested also by previous papers on flow separation and eddy formation [e.g. *Signell and Geyer* 1991]. The quantitative description is made using two main observables which characterize the eddy dimension and intensity respectively similarly to what done in previous works [e.g. *Davies et al.* 1995]. Since the eddy is characterized by a countercurrent in the lee of the cape, with opposite direction with respect to the inflow current, it is useful to consider (see Figure 4):

1. the distance $\hat{X}_c$ between the cape and the downstream coastal point where the countercurrent ends; and

2. the maximum intensity $\hat{U}_m$ reached by the depth-averaged alongshore component of the countercurrent.

In the following the two observables are expressed in non-dimensional form, with the quantities a and U_o being used to normalize length and velocity, respectively, i.e. $X_c = \frac{\hat{X}_c}{a}$ and $U_m = \frac{\hat{U}_m}{U_o}$. For non-stationary flows, averages and standard deviations of (hourly recorded) observables values are computed over time periods τ.

5.1 2D Case

We first examine the results from the benchmark experiments 'C_D2D', (Table 2), which provide information on the sensitivity to the Re_f parameter. Figure 5 shows examples of typical solutions at increasing Re_f. At small Re_f (Re_f=4), the flow tends to follow the coast, and only a small eddy is formed in the lee of the cape. For intermediate Re_f, the eddy remains attached to the cape and it grows in size becoming more elongated. The intensity

of the recirculation remains low, damped by the bottom friction. Finally, for higher values of Re_f ($Re_f > \approx 25$), the eddies detache, and a time-dependent eddy-shedding regime is observed downstream of the cape. In this case, the eddies are relatively small in size, the recirculating flow is intense and the frequency of oscillation is about 2-3 days. These results are consistent with previous numerical [*Davies et al.* 1995] and laboratory experimental results [*Boyer and Tao* 1987].

In Figure 6a, a more quantitative description of the 'C_D2D' experiments is shown, in terms of U_m and X_c as function of Re_f. The critical value $Re_f \simeq 25$ is indicated, beyond which the time-dependent eddy shedding occurs. Before the critical value, the eddy size X_c appears to increase strongly depending on Re_f, while the velocity U_m is almost insensitive and it maintains less than 0.1. The situation changes beyond the critical threshold, where the recirculation intensity increases while X_c maintains almost constant in average.

The dependence of the results on the Rossby number Ro is investigated with the 'U_o2D' experiments (Table 2). In Figure 6b, the results are shown plotting U_m and X_c as a function of Ro at constant Re_f= 17. It is clear that the dependence of the eddy features on the inflow intensity is weak. The countercurrent intensity U_m maintains low for all values of Ro, included the highest value $Ro = 0.8$ corresponding to an unrealistically high cross-shelf transport (approximately twice the typical value of 0.3 Sv in the area). The eddy extension X_c decreases slightly with Ro possibly because bottom friction increases at increasing incoming velocity. Regarding the shape of the inflow current, the experiments with Gaussian cross-shore profiles show negligible differences in comparison with experiments where the inflow is costant. This is probably due to the fact that the phenomenon is controlled by the velocity along the shelf and the slope. There, the action of bottom friction tends to damp the constant incoming velocity on the shelf, creating a profile similar to gaussian.

In summary, the 2D results are in good agreement with previous results. Sensitivity experiments (not shown) have also been carried out considering different, linear parametrizations for bottom friction [e.g. *Döös et al.* 2004]. Results are qualitatively similar to the ones presented here, suggesting that bottom friction is the dominant physical mechanism, independently from the specific parameterization.

5.2 3D Case

The 2D results show that, for the attached eddy regime, the intensity of the recirculation maintains low for the whole parameter range. Only when the eddies detache and propagate, the recirculation intensity grows significantly. This aspect is further examined in the framework of the 3D experiments 'EK_V3D' (Table 2), considering the dependence on vertical eddy viscosity K_M. All the runs have the same Re_f value, $Re_f = 17$, corresponding to the typical coastal value C_D= 0.0025. Two types of stratification (homogeneous and weakly stratified, Table 2) have been considered, and the results appear very similar so that in the following only the weakly stratified case is shown for simplicity.

In Figure 7, a comparison is shown between the depth-averaged velocity and vorticity fields calculated by the 2D model (Figure 7a) and the 3D model for different values of the Ekman number: ($Ek_v = 1.6 \times 10^{-3}$ in Figure 7b and $Ek_v = 1.6 \times 10^{-4}$ in Figure 7c). For high Ek_v, corresponding to high $K_M = 10^{-1}$ m^2/s (not shown), the 3D results approach the 2D results reproducing the low energy attached eddy shown in Figure 7a. As Ek_v decreases, the countercurrent appears to significantly intensify while the eddy extension remains approximately constant (Figure 7b,c).

Plotting U_m and X_c for the experiments 'K_M3D' as function of Ek_v, this trend appears evident (Figure 8a). U_m significantly increases at decreasing Ek_v reaching values of almost order 1, whereas X_c does not change significantly. Furthermore, in the 'U_o3D' experiments, where the dependence on Ro is investigated keeping Re_f and Ek_v constant, we observe that the dependence of X_c is very similar to the 2D case, while the dependence on Ro (Figure 8b) is significantly different from the 2D case (Figure 6b) at least for high Ro. For $Ro = 0.8$, the U_m value in the 3D case increases and more than doubles itself, while in the 2D case U_m shows a deacrease. For $Ro < 0.8$, instead, in both cases U_m appears to deacrease at increasing Ro, even though the 3D values are consistenly higher than the corresponding 2D values.

All together, it appears that in the 3D experiments Re_f is not the only controlling parameter, since Ek_v and at a lesser extent also Ro, play a role in defining the eddy recirculation and in intensifying it .

From the physical point of view, the basic difference between the 2D and 3D dynamics is that in 3D the bottom Ekman layer is explicitely resolved, introducing a vertical shear in the incoming velocity. The relevance of the Ekman layer has been specifically checked running an additional set of experiments characterized by no bottom friction ($C_D = 0$) and high horizontal viscosity $A_M = 50$ m^2/s). In this case, no significant vertical velocity is present and the 2D and 3D results do not show significant differences.

In order to gain a better understanding of the characteristics of the shear flow and of the mechanisms that link it to the recirculation intensification, we consider vertical sections of the three components of the velocity at different locations (indicated in Figure 7b) for the case of $Ek_v = 1.6 \times 10^{-3}$ (i.e. $K_M = 10^{-2}$ m^2/s).

On the shelf upstream of the cape (transect A), the classical bottom Ekman layer strucure can be seen (Figure 9), characterized by reduced flow in the alongshore direction and by a well defined cross-shore transport directed offshore and associated with a downwelling pattern. This is consistent with the expected dissipation mechanism of negative vorticity present on the shelf and the values calculated by the model qualitatively agree with the theoretical estimate of the boundary layer amplitude [*Pedlosky* 1987] $\delta_E \approx 7$ m and of the Ekman suction velocity [*Gill* 1982] $w_E \approx 10^{-3}$ m/s. Notice that in the upper layers a less intense flux toward the coast develops and the elevation profile drops slightly near the coast.

At the eastern corner of the cape (transect B), where the flow tends to detach from the cape (Figure 10), the cross-shore component of velocity is directed toward the open sea from the surface to the bottom, the vertical component is negative and in the elevation profile it is clear the minimum of pressure already observed in Figure 4.

Downstream of the cape (transect C), the bottom Ekman layer is restablished (Figure 11) and within it the offshore transport and the downwelling vertical velocity. The interesting point, though, is that in the surface layers above the Ekman layer a well defined inshore transport is noticeable, associated with an upwelling region close to the shelf break. The inshore velocity reaches the intensity of about 5 cm/s, while the vertical velocity is about 1.5 mm/s. It is this inshore current that appears responsable for the observed gyre intensification.

A possible mechanism for the observed inshore surface transport is provided by the known phenomenon of "secondary circulation" developed in the transverse plane by a vertically sheared curving current [e.g. *Rovzoski* 1957; *Kalkwijk and Booij* 1986; *Geyer* 1993]. When an incoming current with vertically varying velocity develops a curvature, the centrifugal and Coriolis accelerations (which vary with depth as function of the along velocity) tend to be locally imbalanced with respect to the pressure gradient in the cross-stream direction. In energetic flows at high Ro the centrifugal effects dominate, and an offshore surface transport develops due to the centrifugal force "excess" in the faster upper layers. Opposite, inshore transport occurs in the lower layer. Secondary circulations of this type have been observed in tidal flows around a cape [*Geyer* 1993], and they result in a "smearing" of the horizontal shear and a weakening of the vorticity of the depth-averaged recirculation.

In our case the situation is different, since $Ro < 1$ and the Coriolis effect appears to be dominant. For anticyclonic curvature, the Coriolis effect is expected to create an inshore surface transport, that tends to sharpen the horizontal shear and to intensify the vorticity of the depth-averaged recirculation. This is consistent with the observed vertical shear (Figure 11) and with the eddy intensification. An a-priori estimate of the secondary current strength v is not easy to compute, given the sensitivity to the mixing and to the vertical structure of the incoming current. Nevertheless, an order of magnitude estimate based on analytical results of *Kalkwijk and Booij* [1986] suggests $v \approx 3fH_o \approx 7$ cm/s, which is of the same order as the observed inshore velocity. It is also interesting to notice that in our case the secondary circulation appears associated with a downwelling/upwelling pattern, consistently with what suggested by *Garrett and Loucks* [1976]. The inshore surface flow tends to supply the offshore bottom flow by downwelling in the area close to the coast, while the vertical cell tends to be closed by upwelling near the shelf break. The steep slope acts as a dynamical wall, determining the size of the recirculation. This is clearly illustrated in Figure 12b, where a map of the upwelling and downwelling pattern at 25 m is shown. Figure 12a provides a horizontal view of the veering of the current with depth, further illustrating the size and extension of the secondary circulation.

6 Experiments with Realistic Bathymetry

6.1 Numerical Setup

The numerical setup for realistic bathymetry is the same as for the idealized bathymetry, in terms of model integration and boundary conditions (see §4). Coastline and bathymetry data were downloaded by the web sites http://rimmer.ngdc.noaa.gov/coast/getcoast.html and http://pdas.navo.navy.mil, respectively. They have been interpolated on a 200×100 rectangular mesh grid, rotated of 27 degree anticlockwise with respect the true north, using SEAGRID MatLab tools (http://woodshole.er.usgs.gov/staffpages/cdenham/public_html/seagrid/seagrid.html). The horizontal resolution varies linearly both in the alongshore and in the cross-shore directions: $336 \leq \Delta x \leq 2017\,\mathrm{m}$, $225 \leq \Delta y \leq 1737\,\mathrm{m}$. The minimum grid spacing is inshore at the cape and the maximum grid spacing is in the southwest and southeast corners. The vertical resolution is 31 sigma layers.

Beginning from 500-m isobath the topography is drastically simplified assuming flat bottom. The open boundaries are placed far enough away from the domain of interest to avoid interfering with the flow around the cape. To facilitate this, 25 grid meshes with constant cross-shore bathymetry profile, are added both at the eastern and western boundaries. Therefore the total dimensions of the numerical domain are $89 \times 49\,\mathrm{km}$.

To respect the criterion $\left|\frac{\sigma}{H}\frac{\partial_y H}{\partial \sigma}\right| < 1$ [*Mellor et al.* 1994, 1998], a refined σ grid near the bottom was adopted and the bathymetry was smoothed with *ad hoc* programs. Following the Courant-Friedrichs-Lewy criterion, the external and internal time steps were set to $\Delta te = 1\,\mathrm{s}$ and $\Delta ti = 30\,\mathrm{s}$, respectively.

6.2 Results

A set of preliminary experiments have been carried out considering similar parameter ranges as for the idealized experiments. The results are consistent with the ones in §5, even though the realistic topography experiments appear to be slightly more viscous than the idealized ones at given friction parameters. This is probably due to both the roughness of the real topography and to the shallower bathymetry present in the two gulfs adjacent to the

Promontorio of Portofino, with respect to the idealized topography.

The experiment results have been qualitatively compared with the measurement results (Figure 2), considering mean velocity values from current meters (Table 1) and model velocities in analogous locations. Since the model setup is very simple and the measurements are sparse, the comparison is purely qualitative. It aims to verify whether or not the model can reproduce the observed circulation pattern and the order of magnitude of the measured velocity.

Results of the 2D experiments show that the 2D model is not able to reproduce the measurement results, for any of the considered parameters. For the attached eddy regime, the recirculation intensity always underestimates the data of almost an order of magnitude. For the eddy-shedding regime, the recirculation intensifies reaching realistic values, but the eddies propagate with a periodicity of 2-3 days inducing fluctuation and reversal in the downstream model velocity. Such reversals with periods of a few days are not observed in the downstream current measurements, characterized by more persistent velocity direction.

In contrast with the 2D results, 3D experiments appear able to reproduce the basic characteristics of the observed current for appropriate values of the K_M coefficient. As discussed in §5 for the idealized bathymetry experiments, this is related to the presence of vertical shear induced by the resolved bottom Ekman layer, which allows for a tightening and intensification of the attached eddy. The vertical shear structure and upwelling/downwelling patterns are similar to those discussed in §5 for the idealized experiments.

A visual comparison of 2D and 3D results is shown in Figure 13 for realistic values of bottom friction coefficient (C_D=0.0025) and incoming velocity (U_e=25 cm/s). For the 3D case, $K_M = 10^{-3}$ m^2/s is considered, corresponding to $Ek_v = 1.6 \times 10^{-4}$.

As it can be seen, the 2D results show a very weak recirculation in the lee of the cape (Figure 13a). The current intensity calculated in the location corresponding to the Camogli current meter is $\approx$ 0.3 cm/s, i.e. an order of magnitude smaller than the measured one which is of the order of 2.5 cm/s (Table 1). Notice that the model velocity is lower than the measured one also at the upstream Sestri Levante location (Table 1), by almost a factor 2. This suggests that the friction parameter might be too high. On the other hand, when

decreasing C_D, the eddy becomes unrealistically elongated with respect to the data (which suggest $\hat{X}_c < 15$ km), and the recirculation intensity remains unrealistically low. Similar results are obtained also with different linear parameterizations of bottom friction. In other words, as mentioned above, the 2D model appears lacking of the correct mechanism to reproduce the eddy intensification, so that no parameter fitting allows to recover the observed velocity values.

In the 3D results (Figure 13b) the recirculation is clearly intensified and also the detachement pattern from the cape is more evident. The model current velocities at the Camogli and Sestri locations are ≈ 5 cm/s and ≈ 25 cm/s respectively, in qualitative agreement with the measured values (Table 1). Also the eddy size appears realistic, as indicated by the fact that the model current at the Bogliasco location is in the same northwestard direction as for the measurements and with similar intensity.

7 Summary and Concluding Remarks

In this paper, a process study is presented aimed at investigating the winter circulation in the area of the Promontorio of Portofino. Information on the circulation are provided by historical measurements from three current meters, one located upstream of the cape and two downstream. The measurements are not contemporaneous and they are used to infer only qualitative information on the current patterns. They indicate that the incoming current on the shelf is in the northwestern direction and is highly persistent in time. Behind the cape, a southwestward recirculation is observed, suggesting the existence of an attached anticyclonic eddy with intensity $\approx 10\%$ of the incoming shelf current and with extension < 15 km.

The process study is first performed considering an idealized bathymetry consisting of a narrow shelf with a steep slope and a quadrangular cape, whose parameters are based on the realistic topography. A steady current entering from the eastern boundary of the domain is prescribed and its interaction with the cape is studied. Numerical experiments are performed using both 2D (vertically integrated) and 3D versions of the POM model, investigating the sensitivity to environmental parameters.

The 2D results are consistent with previous numerical and experimental results [*Pattiaratchi et al.* 1986; *Signell and Geyer* 1991; *Davies et al.* 1995; *Denniss et al.* 1995] obtained in the literature with simpler and shallower topography. The main controlling parameter appears to be the equivalent Reynolds number Re_f, given by the ratio between advection and bottom friction terms. For small Re_f, when the bottom friction coefficient C_D is high (or equivalently the depth H_o is shallow) the flow tends to follow the coast. For intermediate Re_f, an attached recirculating eddy forms in the lee of the cape, becoming more elongated at increasing Re_f while the intensity of the recirculation remains low. For Re_f greater than a critical value, a time-dependent eddy-shedding regime is observed, characterized by relatively small and intense eddies propagating along the shelf downstream of the cape. These results appear quite insensitive to the values of the Rossby number, i.e. to the intensity of the incoming current.

In the 3D case, other two adimensional parameters come to play, i.e. the Burger number Sb quantifying the stratification effects and the Ekman vertical number Ek_v, quantifying vertical mixing effects. Two different cases of stratifications are considered, homogeneous and weakly stratified, and the results appear basically unchanged. The dependence on Ek_v is investigated varying the vertical viscosity K_M at fixed Re_f. The Re_f value is realistic and it corresponds to an attached eddy regime. For values of K_M in a realistic range, the 3D solutions show a significant intensification of the attached eddy with respect to the 2D solutions, while the eddy size is basically unchanged. Also, a greater dependence on the Rossby number Ro is noticed.

The main difference between the 2D and 3D dynamics is the presence of a resolved bottom Ekman layer in 3D, introducing a vertical shear in the incoming current. In the bottom Ekman layer, the current is weakened in the alongshore direction while a cross-shore component is formed with a net transport directed offshore and associated with a downwelling pattern, consistent with the dissipation of negative vorticity on the shelf. In the region where the downstream eddy forms, a noticeable cross-shore current is present also in the surface layers. This current is directed inshore, i.e. opposite to the bottom Ekman transport, and is associated with an upwelling vertical velocity at the shelf break. The inshore current appears

responsable for the observed eddy intensification.

A possible mechanism for the observed inshore surface transport is given by the known phenomenon [e.g. *Rovzoski* 1957; *Kalkwijk and Booij* 1986] of formation of a "secondary circulation" (in the transverse plane) associated with a curving current with vertically sheared velocity. The secondary current is due to a local imbalance between the cross-stream pressure gradient and the centrifugal and Coriolis accelerations. In our simulations, differently from previous observation in the literature [*Geyer* 1993], the Coriolis effect appears dominant, since $Ro < 1$. For an anticyclonic circulation, the "excess" of Coriolis force in the faster upper layers determines an inshore surface transport which tends to intensify the vorticity of the depth-averaged recirculation. The inshore current is supplemented by the upwelling region close to the shelf break, resulting in a vertical cell. The presence of the slope is likely to confine the phenomenon, since the effects of vertical shear become less prominent with increasing depth [e.g. *Jacobs et al.* 1998].

Experiments with realistic bathymetry are then performed, and the numerical results are qualitatively compared with the current meter measurement results. For the 2D case, the model does not seem to be able to reproduce the measurement results, for any of the considered parameters. For values of Re_f corresponding to the attached eddy regime, the recirculation intensity always underestimates the measurements by approximately an order of magnitude. For the eddy-shedding regime, fluctuations with periodicity of a few days occur in the model downstream velocity, which are not present in the current meter data. The 3D results, instead, show a good qualitative agreement with the measurement results for realistic values of the parameters. The attached eddy intensifies with respect to the 2D case, reaching realistic values of recirculating velocity and its extension is less than 15 km, in agreement with what suggested by the measurements.

These results can have significant consequences from the point of view of transport and response of biological quantities. They indicate the presence of a mechanism which, when vertical shear is significant, determines an inshore surface transport downstream the cape, associated with upwelling events in a region which would otherwise be downwelling dominated. The inshore transport and the intensification of the attached eddy can alter the biological

response through particle entrapping and retention [e.g. *Coutis and Middleton* 1999], while the presence of upwelling is expected to directly influence biological productivity. Notice that this mechanism is directly related to the topography of the shelf and of the slope, and it would not be present in a shallow environment, where vertical homogenization tends to occurr, nor in very deep water, where the effects of the bottom Ekman layer are negligible [*Coutis and Middleton* 2002]. The actual generality and time persistency of the phenomenon are not yet assessed at this stage. There are many effects that could contribute to alter it, such as the effects of stratification, local atmospheric forcings and time variability in the incoming current [e.g. *Aiken et al.* 2002]. Further investigations, in terms of both numerical modelling and field measurements, will be necessary to assess this point.

The present results also provide some useful insights for future more realistic modelling. Vertical shear and vertical mixing appear to be important ingredients that can have a first order impact on the setting of horizontal recirculation structures. As a consequence, they have to be correctly modelled, even for applications aimed at reproducing depth average velocity patterns. This suggests that 2D models might not be appropriate for the Promontorio di Portofino area, and possibly more in general for regions with complex topography and steep slope. Regarding vertical mixing coefficients, the present results suggest that values of $K_M \approx 10^{-3}$ m^2/s are appropriate, at least for the considered winter conditions. It is important to remark, though, that in this study, a simple constant vertical viscosity K_M has been considered (since we are interested in a sensitivity study where the impact of changing K_M is investigated). For future applications, on the other hand, more complex mixing parameterizations should be used, able to provide estimates of K_M as function of environmental parameters [e.g. *Durski et al.* 2004]. More numerical investigations [e.g. *Wijesekera et al.* 2003] and better data coverage will be necessary to quantitatively test the results.

Acknowledgments

The authors wish to thank R. Festa, M. Iskandarani, G. Gasparini, Z. Garraffo, T. Ozgokmen and G. Sannino for many interesting conversations and useful suggestions. We also thank Antonio Schirone for his assistance with the SIAM database of the Italian National Agency

for New Technologies, Energy and Environment (ENEA). A. M. Doglioli was supported by the Università degli Studi di Genova, Contract 182 26.10.2000 GEO/02-FIS/02, (PI's Roberto Festa and Sergio Tucci), while A. Griffa was supported by the Consiglio Nazionale delle Ricerche (CNR) and the Office of Naval Research (ONR), grant N00014-97-1-0620. We also wish to acknowledge the support provided by the the Istituto Nazionale Fisica della Materia (INFM) and in particular by Corrado Ratto.

References

Aiken, C., A. Moore, and J. Middleton, The nonnormality of coastal ocean flows around obstacles and their response to stochastic forcing, *J. Phys. Oceanogr.*, *32*(10), 2955–2974, 2002.

Aliani, S., A. Griffa, and A. Molcard, Floating debris in the Ligurian Sea, North-Western Mediterranean, *Mar. Poll. Bull.*, *46*, 1142–1149, 2003.

Astraldi, M., and G. Gasparini, La circolazione costiera nel Mar Ligure orientale, *Boll. Mus. Ist. Biol. Univ. Genova*, *52 suppl*, 317–331, 1986.

Astraldi, M., and G. Manzella, Some observations on current measurements on the East Ligurian shelf, Mediterranean Sea, *Cont. Shelf Res.*, *2*, 183–193, 1983.

Astraldi, M., G. Gasparini, and G. Manzella, Temporal variability of currents in the Eastern Ligurian Sea, *J. Geophys. Res.*, *95(C2)*, 1515–1522, 1990.

Bastos, A., N. Kenyon, and M. Collins, Sedimentry processes, bedforms and facies, associtated with a coastal headland: Portland Bill, Southern UK, *Mar. Geol.*, *187*(3-4), 235–258, 2002.

Bastos, A., M. Collins, and N. Kenyon, Water and sediment movement around a coastal headland: Portland Bill, Southern UK, *Ocean Dynamics*, *53*(3), 309–321, 2003.

Batchelor, G., *An Introduction to Fluid Dynamics*, Cambridge University Press, London and New York, 1967.

Black, K., and S. Gay, Eddy formation in unsteady flows, *J. Geophys. Res.*, *92*, 9514–9522, 1987.

Blumberg, A., and G. Mellor, A description of a three-dimensional coastal ocean circulation model, in *Three-Dimensional Coastal Ocean Models*, vol. 4, edited by N. Heaps, p. 208, American Geophysical Union, Washington, D.C., 1987.

Boyer, D., and L. Tao, On the motion of linearly stratified rotating fluids past capes, *J. Fluid Mech.*, *180*, 429–449, 1987.

Brooks, D., Currents at Lindenkohl Sill in the southern Gulf of Maine, *J. Geophys. Res.*, *95*(C12), 22,173–22,192, 1990.

Buffoni, G., P. Falco, A. Griffa, and E. Zambianchi, Dispersion processes and residence times in a semi-enclosed basin with recirculating gyres. An application to the Tyrrhenian Sea, *J. Geophys. Res.*, *102*(C8), 18699–18713, 1997.

Castellari, S., N. Pinardi, and K. Leanman, Simulation of water mass formation processes in the Mediterranean Sea: Influence of the time frequency of the atmospheric forcing, *J. Geophys. Res.*, *105*(C10), 24157–24181, 2000.

Cattaneo Vietti, R., A. Sirigu, and A. Tommei, *Sea of Liguria*, 1-162 pp., Ed. Centro Studi Unione Camere di Commercio Liguri, Genova, 1982.

Chapman, D., Numerical treatment of cross-shelf open boundaries in a barotropic coastal ocean model, *J. Phys. Oceanogr.*, *8*, 1060–1075, 1985.

Chiswell, S., and D. Roemmich, The east cape current and two eddies: a mechanism for larval retention?, *N. Z. J. Mar. Freshwat. Res.*, *32*(3), 385–397, 1998.

Coutis, P., and J. Middleton, Flow-topography interaction in the vicinity of an isolated deep ocean island, *Deep Sea Res.I*, *46*, 1633–1652, 1999.

Coutis, P., and J. Middleton, The physical and biological impact of a small island wake in the deep ocean, *Deep Sea Res.I*, *49*, 1341–1361, 2002.

Davies, P., J. Dakin, and R. Falconer, Eddy formation behind a coastal headland, *J. Coast. Res.*, *11*(1), 154–167, 1995.

Denniss, T., J. Middleton, and R. Manasseh, Recirculation in the lee of complicated headlands: A case study of Bass Point, *J. Geophys. Res.*, *100*(C8), 16,087–16,100, 1995.

Doglioli, A., M. Magaldi, L. Vezzulli, and S. Tucci, Development of a numerical model to study the dispersion of wastes coming from a marine fish farm in the Ligurian Sea (Western Mediterranean), *Aquaculture*, *231*(1-4), 215–235, 2004.

Döös, K., J. Nycander, and P. Sigry, Slope-dependent friction in a barotropic model, *J. Geophys. Res.*, *109, C01008, doi:10.1029/2002JC001517*, 2004.

Durski, S., S. Glenn, and D. Haidvogel, Vertical mixing schemes in the coastal ocean: Comparison of the level 2.5 Mellor-Yamada scheme with an enhanced version of the K-profile parameterization, *J. Geophys. Res.*, *109, C01015, doi:10.1029/2002JC001702*, 2004.

Esposito, A., and G. Manzella, Current circulation in the Ligurian Sea, in *Hydrodynamics of semi-enclosed seas*, edited by J. Nihoul, pp. 187–204, Elsevier Scientific Publishing Company, Amsterdam, 1982.

Farmer, R., D. Pawlowicz, and R. Jiang, Tilting separation flows: a mechanism for intense vertical mixing in the coastal ocean, *Dyn. Atmos. Oceans*, *36*, 43–58, 2002.

Ferentinos, G., and M. Collins, Effects of shorelines irregulaties on a rectilinear tidal current and their significance in sedimentation processes, *J. Sedim. Petrol.*, *50*, 1081–1094, 1980.

Flather, R., A tidal model of the northwest European continental shelf, *Mem. Soc. R. Sci. Liege*, *Ser. 6*(10), 141–164, 1976.

Freeland, H., The flow of a coastal current past a blunt headland, *Atmosphere-Ocean*, *28*, 288–302, 1990.

Garrett, C., and R. Loucks, Upwelling along the tarmouth shore of Nova Scotia, *J. Fish. Res. Board of Can.*, *33*, 116–117, 1976.

Geyer, W., Three-dimensional tidal flow around headlands, *J. Geophys. Res.*, *98*(C1), 955–966, 1993.

Gill, A. E., *Atmophere-Ocean Dynamics*, Academic Press, New York, 1982.

Haidvogel, D., and Beckmann, Numerical models of the coastal ocean, in *The sea*, vol. 10, edited by K. Brink and A. Robinson, pp. 457–482, John Wiley & Sons,Inc., 1998.

Jacobs, P., Y. Guo, and P. Davies, Boundary currents over shelf and slope topography, *J. Mar. Sys.*, *19*, 137–158, 1998.

Kalkwijk, J., and R. Booij, Adaptation of secondary flow in nearly-horizontal flow, *J. Hydraul. Eng.*, *24*, 19–37, 1986.

Mellor, G., *Users Guide for a three-dimensional, primitive equation, numerical ocean model.*, Princeton University, Princeton, NJ 08544-0710, 1998.

Mellor, G. L., T. Ezer, and L.-Y. Oey, The pressure gradient conudrum of sigma coordinate ocean models, *J. Atmos. Oceanic Technol.*, *11*, 1126–1134, 1994.

Mellor, G. L., L.-Y. Oey, and T. Ezer, Sigma coordinate pressure gradient errors and the seamount problem, *J. Atmos. Oceanic Technol.*, *15*, 1122–1131, 1998.

Merkine, L., Flow separation on a β-plane, *J. Fluid Mech.*, *99*, 399–409, 1980.

Merkine, L., and A. Solan, The separation of flow past a cylinder in a rotating system, *J. Fluid Mech.*, *92*, 381–392, 1979.

Molcard, A., N. Pinardi, M. Iskandarani, and D. Haidvogel, Wind driven general circulation of the Mediterranean Sea simulated with a Spectral Element Ocean Model, *Dyn. Atmos. Oceans*, *35*(2), 97–130, 2002.

Orlanski, I., A simple boundary condition for unbounded hyperbolic flows, *J. Comput. Phys.*, *21*, 251–269, 1976.

Palma, E., and R. Matano, On the implementation of passive open boundary conditions for a general circulation model: The barotropic mode, *J. Geophys. Res.*, 1998.

Palma, E., and R. Matano, On the implementation of open boundary conditions for a general circulation model: The three-dimensional case, *J. Geophys. Res.*, 2000.

Pattiaratchi, C., A. James, and M. Collins, Island wakes and headland eddies: a comparison between remotely sensed data and laboratory experiments, *J. Geophys. Res.*, *92*(C1), 783–794, 1986.

Pedlosky, J., *Geophysical Fluid Dynamics*, 2nd ed., Springer-Verlag, New York, 710 pp., 1987.

Pérenne, N., J. W. Lavelle, D. C. Smith IV, and D. L. Boyer, Impulsively started flow in a submarine canyon: Comparison of results from laboratory and numerical models, *J. Atmos. Oceanic Technol.*, *18*, 1698–1718, 2001.

Pingree, R., The formation of the shambles and other banks by tidal stirring of the seas, *J. Mar. Biol. Ass. U.K.*, *58*, 211–226, 1978.

Rovzoski, I., Flows of water in bends of open channels, Jerusalem, Israel Program for Scientific Translation, 1957.

Sadoux, S., J.-M. Baey, A. Fincham, and D. Renouard, Experimental study of the stability of an intermediate current and its interaction with a cape, *Dyn. Atmos. Oceans*, *31*, 165–192, 2000.

Salmona, P., and D. Verardi, The marine protected area of Portofino, Italy: a difficult balance, *Ocean & Coastal Management*, *44*, 39–60, 2001.

Signell, R., and W. Geyer, Transient eddy formation around headlands, *J. Geophys. Res.*, *96*(C2), 2561–2575, 1991.

Smagorinsky, J., General circulation experiments with the primitive equations, I. The basic experiment, *Mont. Weather Rev.*, *91*, 99–164, 1963.

Tansley, C., and D. Marshall, Flow past a cylinder on a beta-plane, with application to Gulf Stream separation and the Antartic Circumpolar Current, *J. Phys. Oceanogr.*, *31*, 3274–3283, 2001.

Verron, J., P. A. Davies, and J. M. Dakin, Quasigeostrophic flow past a cape in a homogeneous fluid, *Fluid Dyn. Res.*, *7*, 1–21, 1991.

Wang, P., J. Martin, and G. Morrison, Water quality and eutrophication in Tampa Bay, Florida, *Estuar. Coast. Shelf Sci.*, *49*(1), 1–20, 1999.

Wijesekera, H., J. Allen, and P. Newberger, Modeling study of turbulent mixing over the continental shelf: Comparison of turbulent closure schemes, *J. Geophys. Res.*, *108(C3), 3103, doi:10.1029/2001JC001234*, 2003.

Wolanski, E., J. Imberger, and M. Heron, Island wakes in shallow coastal waters, *J. Geophys. Res.*, *89*, 10,553–10,569, 1984.

Yankovski, A., and D. Chapman, Generation of mesoscale flows over the shelf and slope by shelf wave scattering in the presence of a stable, sheared mean current, *J. Geophys. Res.*, *100*(C4), 6725–6742, 1995.

Yankovski, A., and D. Chapman, Scattering of shelf waves by a spatially varying mean current, *J. Geophys. Res.*, *101*(C2), 3479–3487, 1996.

Yankovski, A., and D. Chapman, Anticyclonic eddies trapped on the continental shelf by topographic irregularities, *J. Geophys. Res.*, *102*(C3), 5625–5639, 1997.

Position	Period	u *(cm/s)*	u' *(cm/s)*	v *(cm/s)*	v' *(cm/s)*	θ *degree*
Sestri L., 16 m	8-Feb-79 to 30-Apr-79	-37.8	18.0	+0.7	2.4	37
Sestri L., 50 m	8-Feb-79 to 30-Apr-79	-26.6	10.8	+1.7	1.8	33
Sestri L., 95 m	8-Feb-79 to 30-Apr-79	-18.9	9.2	+2.0	1.5	33
Camogli, 10 m	18-Apr-97 to 31-May-97	+2.3	3.9	-0.1	0.8	32
Bogliasco, 29 m	11-Dec-92 to 28-Feb-93	-5.3	5.2	+0.3	1.1	13

Table 1: Statistics of the currents. Mean values (u,v) and standard deviations (u',v') of the alongshore and cross-shore components, respectively. The angle of 'natural' rotation θ is measured clockwise with respect to true north.

Exp.	Ro	Re	Re_f	Ek_v	Sb
C_D2D	0.4	1500	4 - 83	n.d.	n.d.
U_o2D	0.1 - 0.8	360 - 3000	17	n.d.	n.d.
U_o3D	0.1 - 0.8	360 - 3000	17	1.5×10^{-3}	0 - 6.4
K_M3D	0.4	1500	17	1.5×10^{-5}-1.5×10^{-2}	0 - 6.4

Table 2: Parameters variations in numerical experiments. The assignement n.d. (not defined) is used for 3D parameter in 2D experiments.

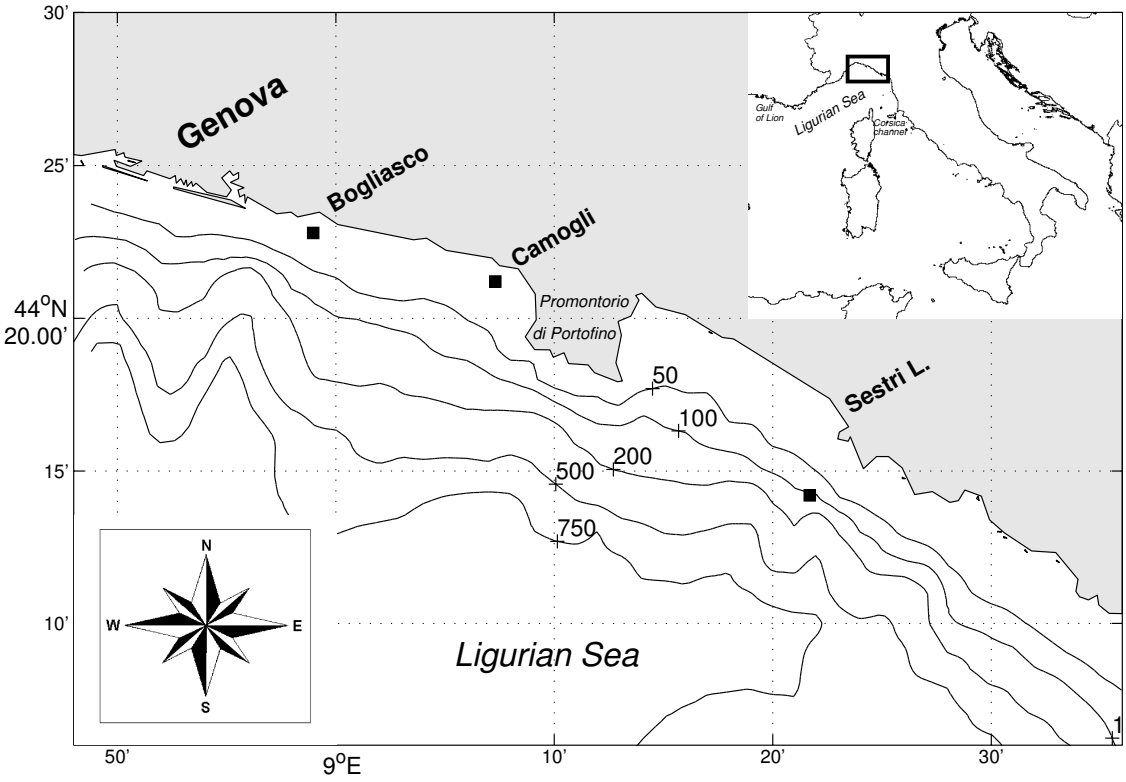

Figure 1: Study area and current meters positions (black squares).

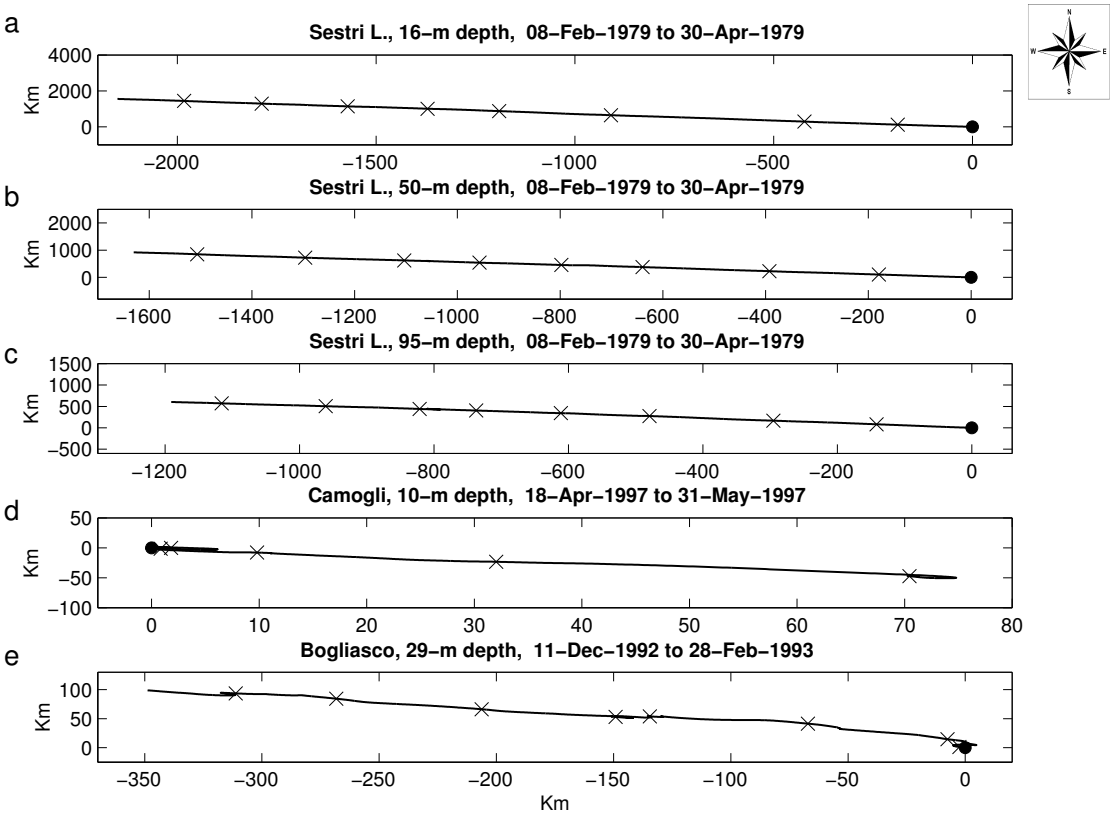

Figure 2: Progressive vector diagrams of current measurements at Sestri Levante, a) 16 m, b) 50 m c) 95 m; d) Camogli, 10 m and e) Bogliasco, 29 m. The crosses represent 10-days intervals and the filled circles point out first data of timeseries.

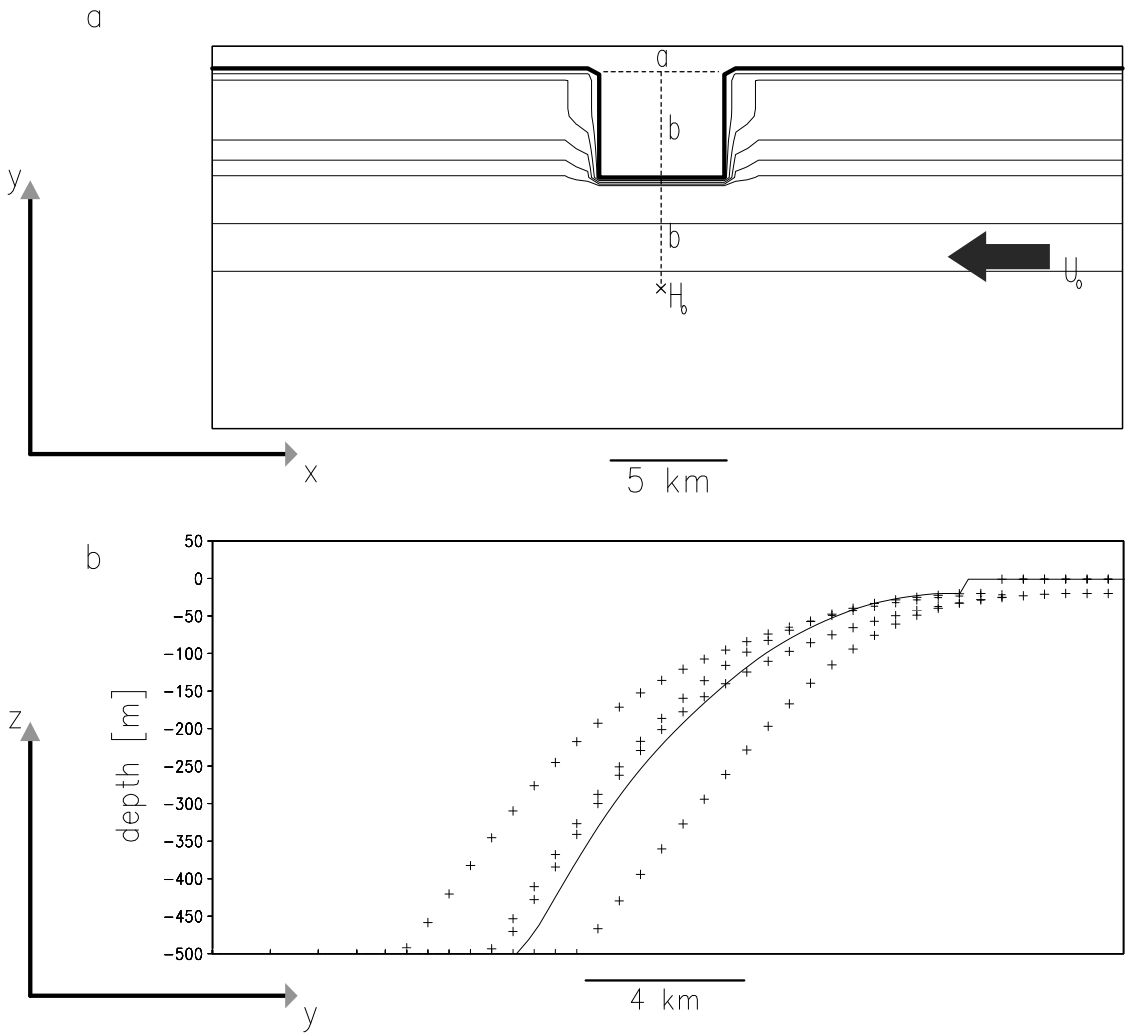

Figure 3: a) Physical system. Bathymetry contour lines at levels 1(coastline in bold) 10 20 30 50 100 200 m. b) Cross-shore profiles comparison between real bathymetry (dotted lines) and idealized bathymetry (solid line).

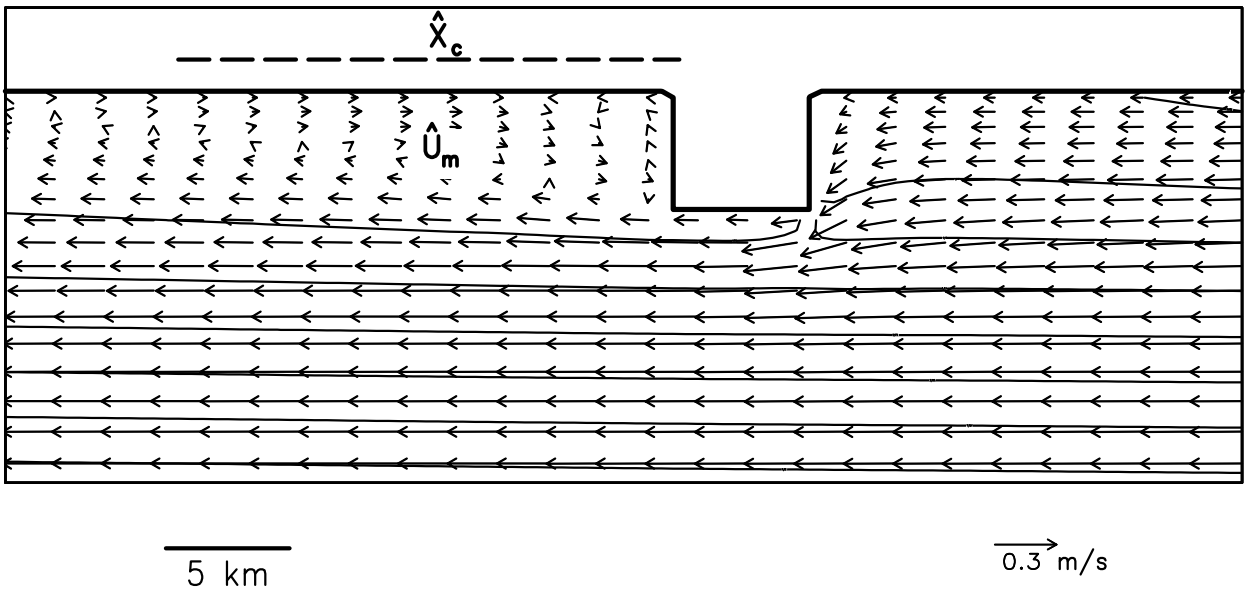

Figure 4: Depth-averaged-velocity vectors and free surface elevation contour lines (contour interval is 4×10^{-3}m) for a typical solution. The observables X_c and U_m are indicated.

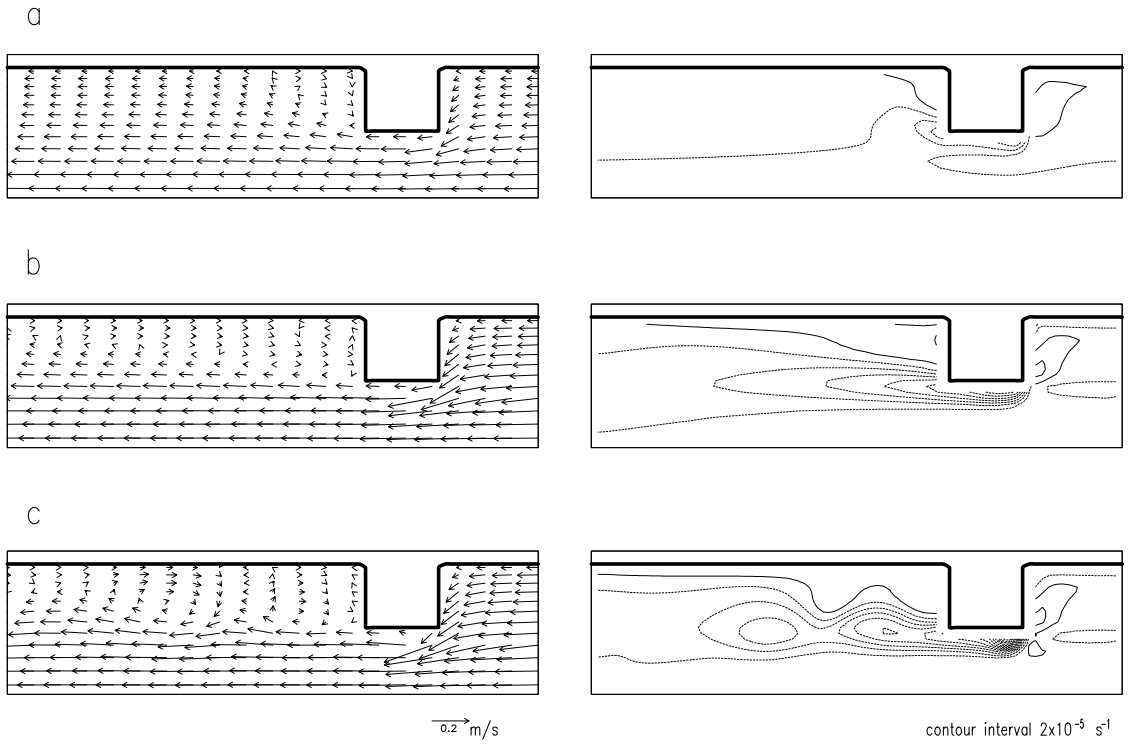

Figure 5: Experiment '$C_D 2D$'. Depth-averaged velocity vectors and depth-averaged vorticity contour lines (the solid contours indicate positive values, the dashed lines indicate negative values) at $\tau = 10$; a) $Re_f = 4$; b) $Re_f = 21$; c) $Re_f = 28$.

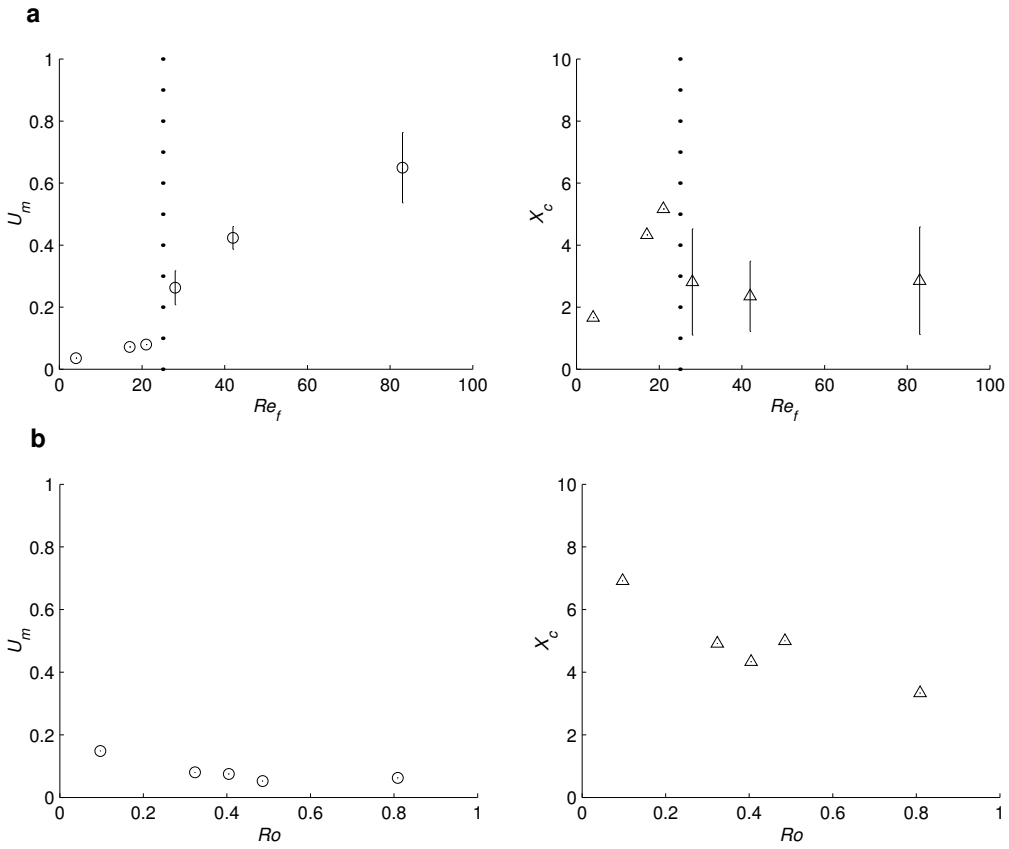

Figure 6: Bidimensional model results. Averages and standard deviation of dimensionless countercurrent intensity U_m (circles) and eddy extention X_c (triangles); a) experiment 'C_D2D'; $9 \leq \tau \leq 10$; the vertical dotted line points out the critical threshold; b) experiment 'U_o2D'; $9 \leq \tau \leq 10$.

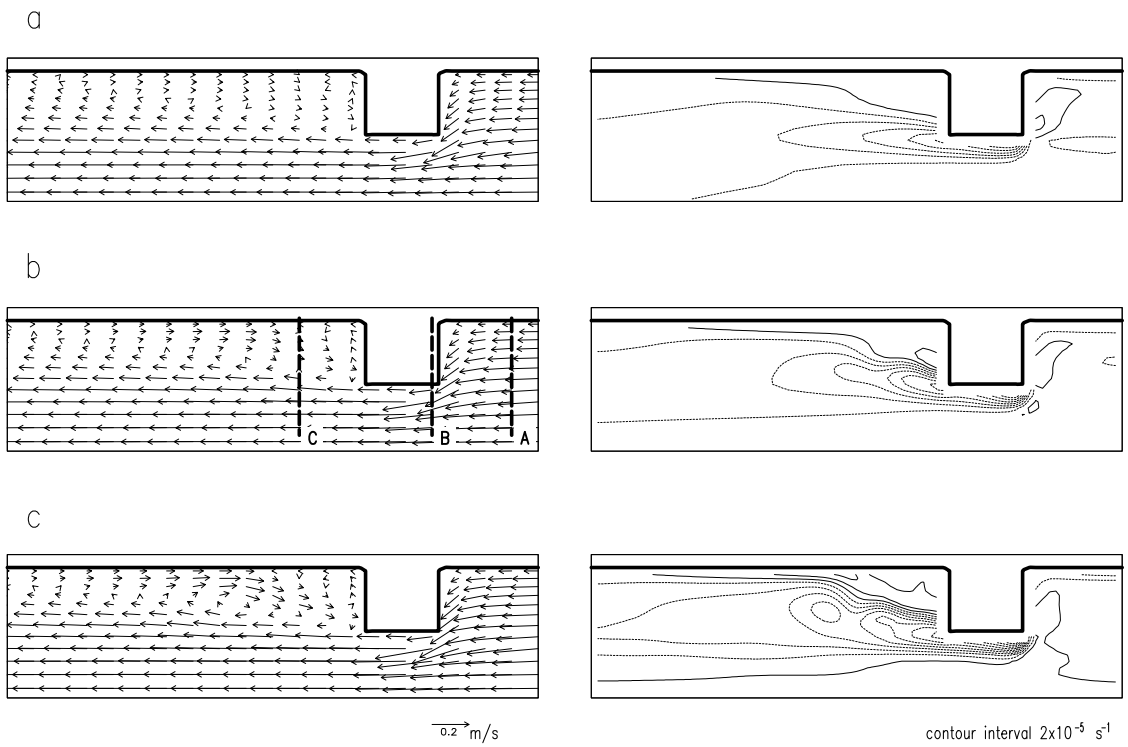

Figure 7: Experiments 'C_D2D' and 'EK_V3D'. Depth-averaged velocity vectors and depth-average vorticity contour lines (the solid contours indicate positive values, the dashed lines indicate negative values) at $\tau = 5$; a) $Sb =$n.d., $EK_v =$n.d. (bidimensional case); b) $Sb = 6.4$, $EK_v = 1.6 \times 10^{-3}$; c) $Sb = 6.4$, $EK_v = 1.6 \times 10^{-4}$. The long dashed lines in b) show the position of cross-shore sections of Figure 9 (A), Figure 10 (B), Figure 11 (C).

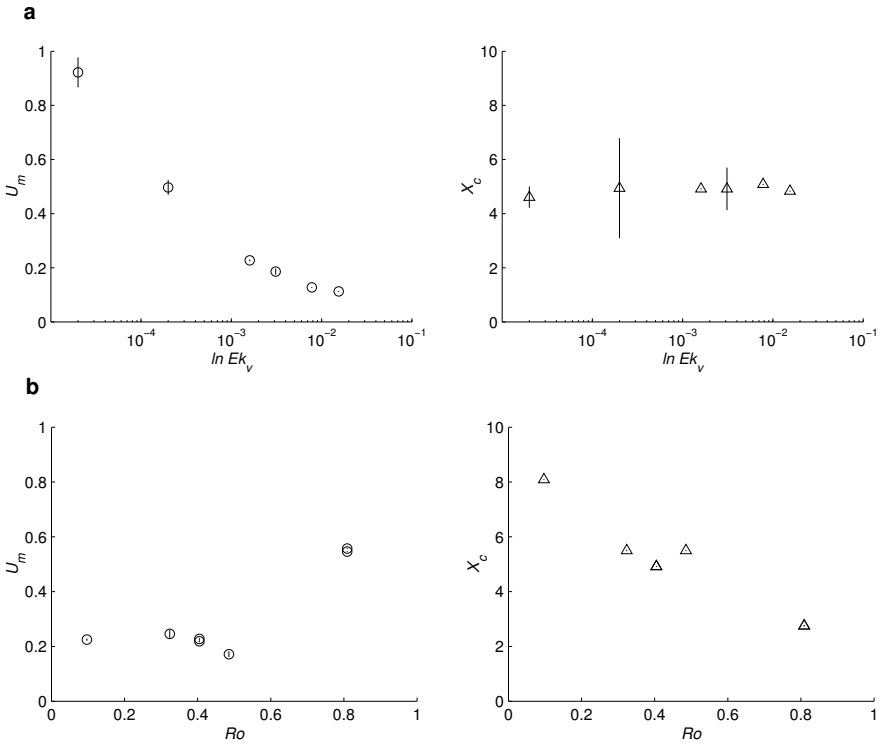

Figure 8: Threedimensional model results. Averages and standard deviation of dimensionless countercurrent intensity U_m (circles) and eddy extention X_c (triangles); a) Experiment '$K_M 3D$'; $4 \leq \tau \leq 5$; b) Experiment '$U_o 3D$'; $4 \leq \tau \leq 5$.

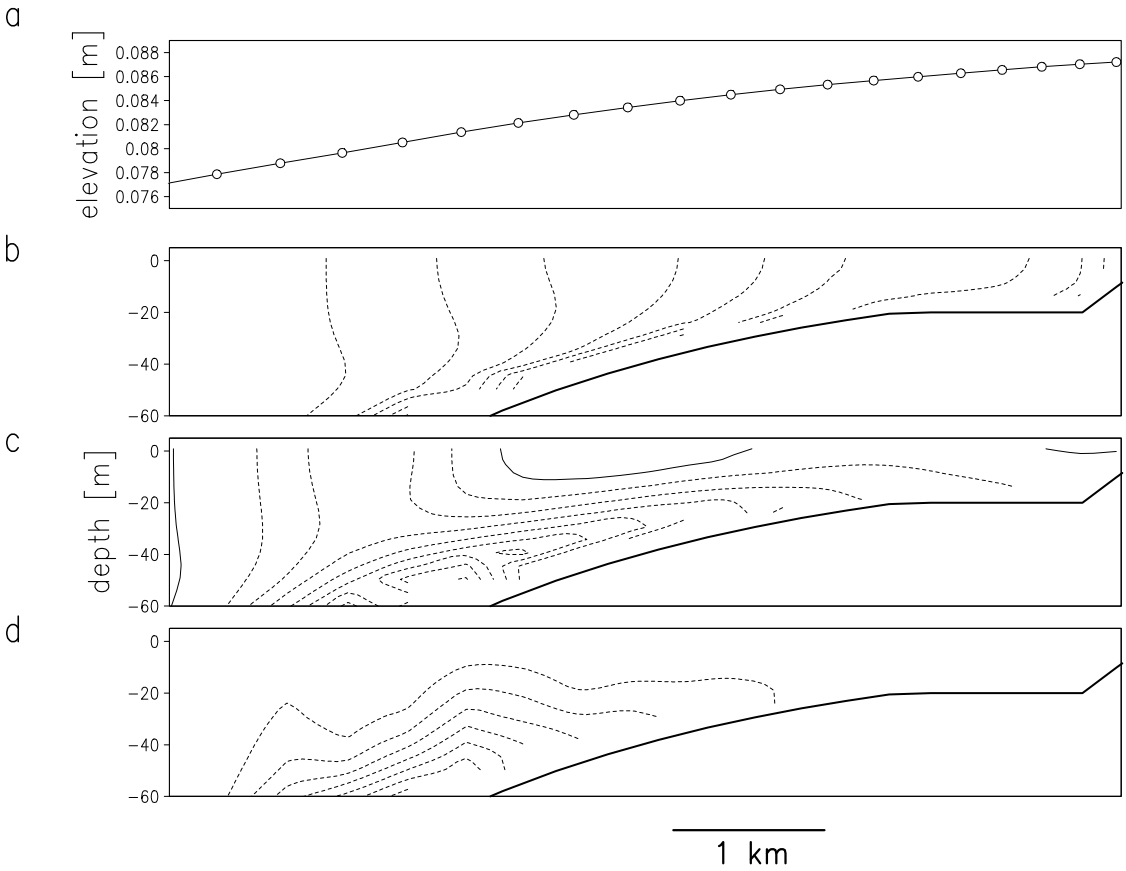

Figure 9: Cross-shore transect A from Figure 7. Experiment '$K_M 3D$'; $\tau = 5$. a) profile of free surface elevation and vertical sections of b) alongshore, c) cross-shore and d) vertical component of velocity. The solid contours indicate positive values, the dashed lines indicate negative values and contour interval is b) 0.02 c) 0.005 d) 0.0003 m/s.

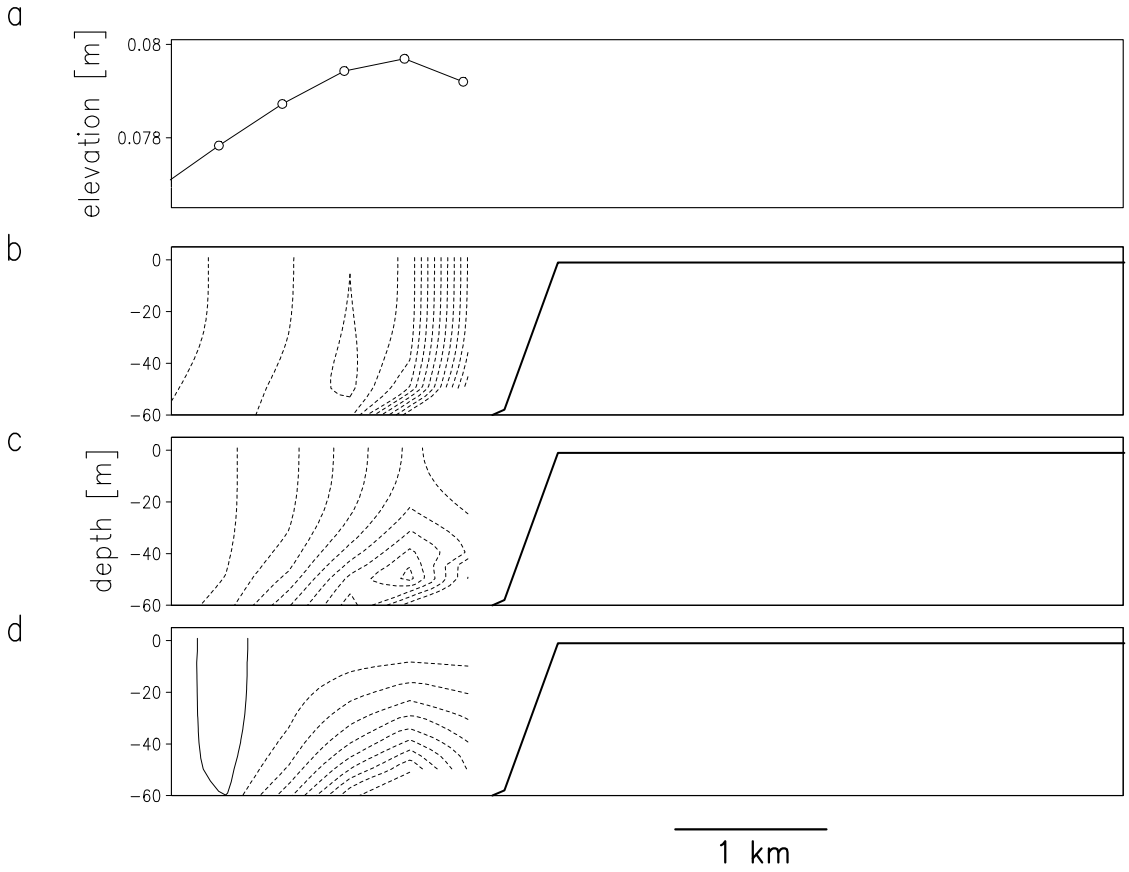

Figure 10: Cross-shore transect B from Figure 7. Panels as in Figure 9.

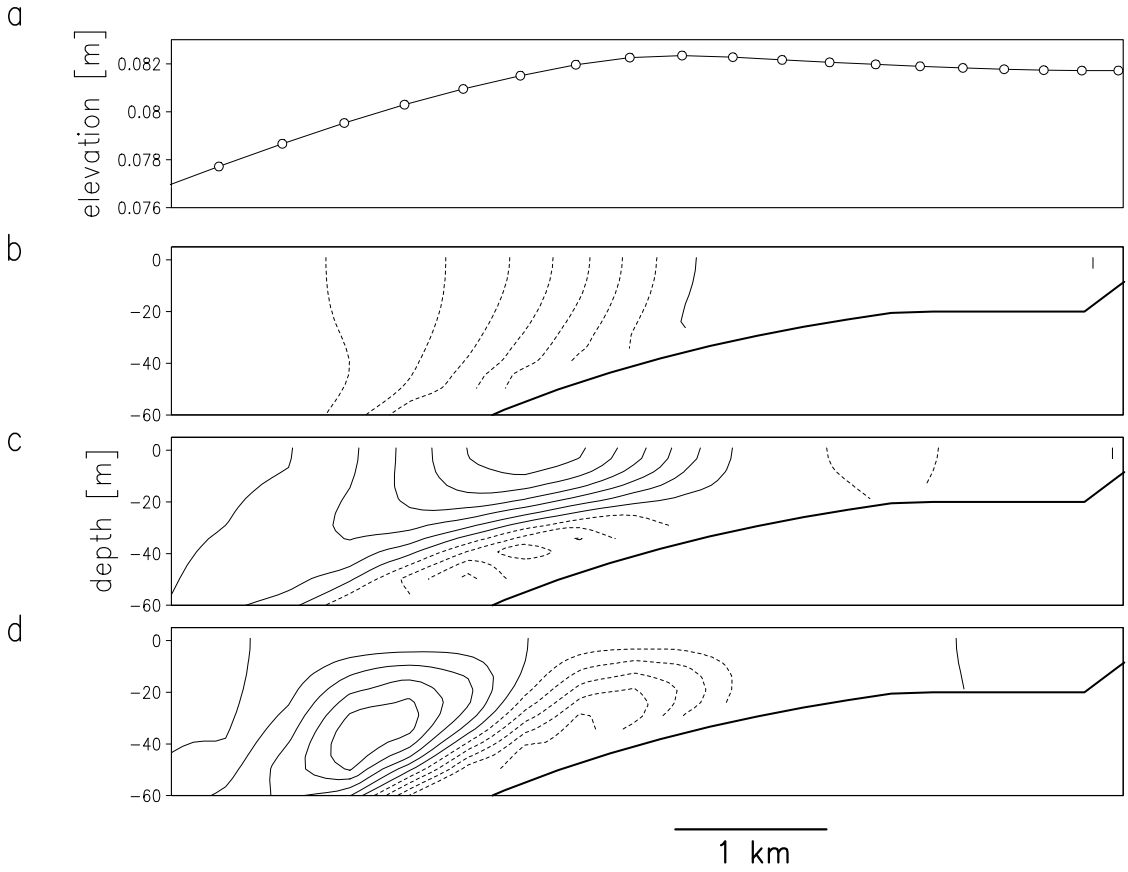

Figure 11: Cross-shore transect C from Figure 7. Panels as in Figure 9.

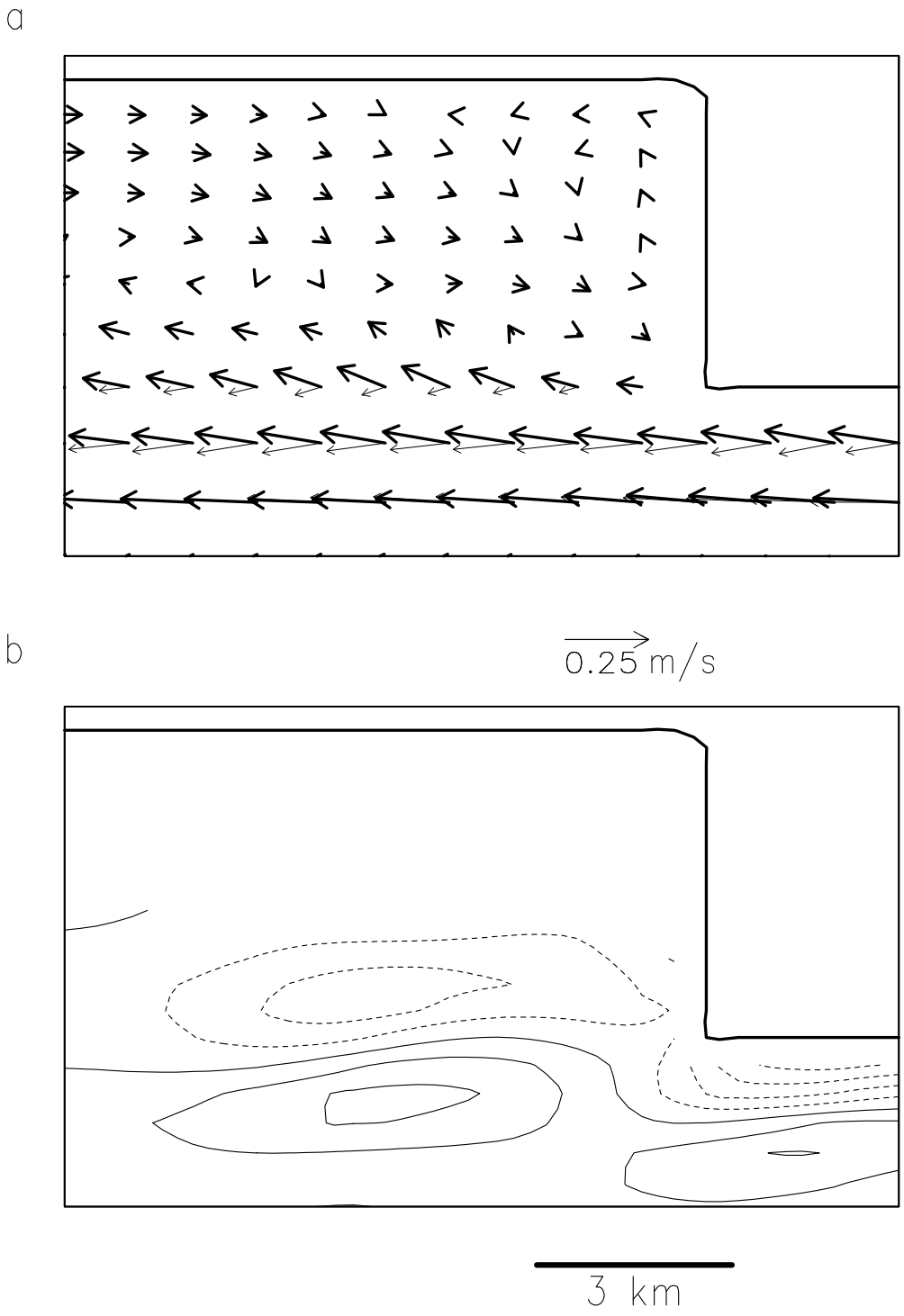

Figure 12: Experiment '$K_M 3D$'; $\tau = 5$. a) Velocity vectors at 1 m (bold) and at 50 m (thin). b) Vertical velocity at 25 m contour line. The solid contours indicate positive values, the dashed lines indicate negative values and contour interval is 0.0003 m/s.

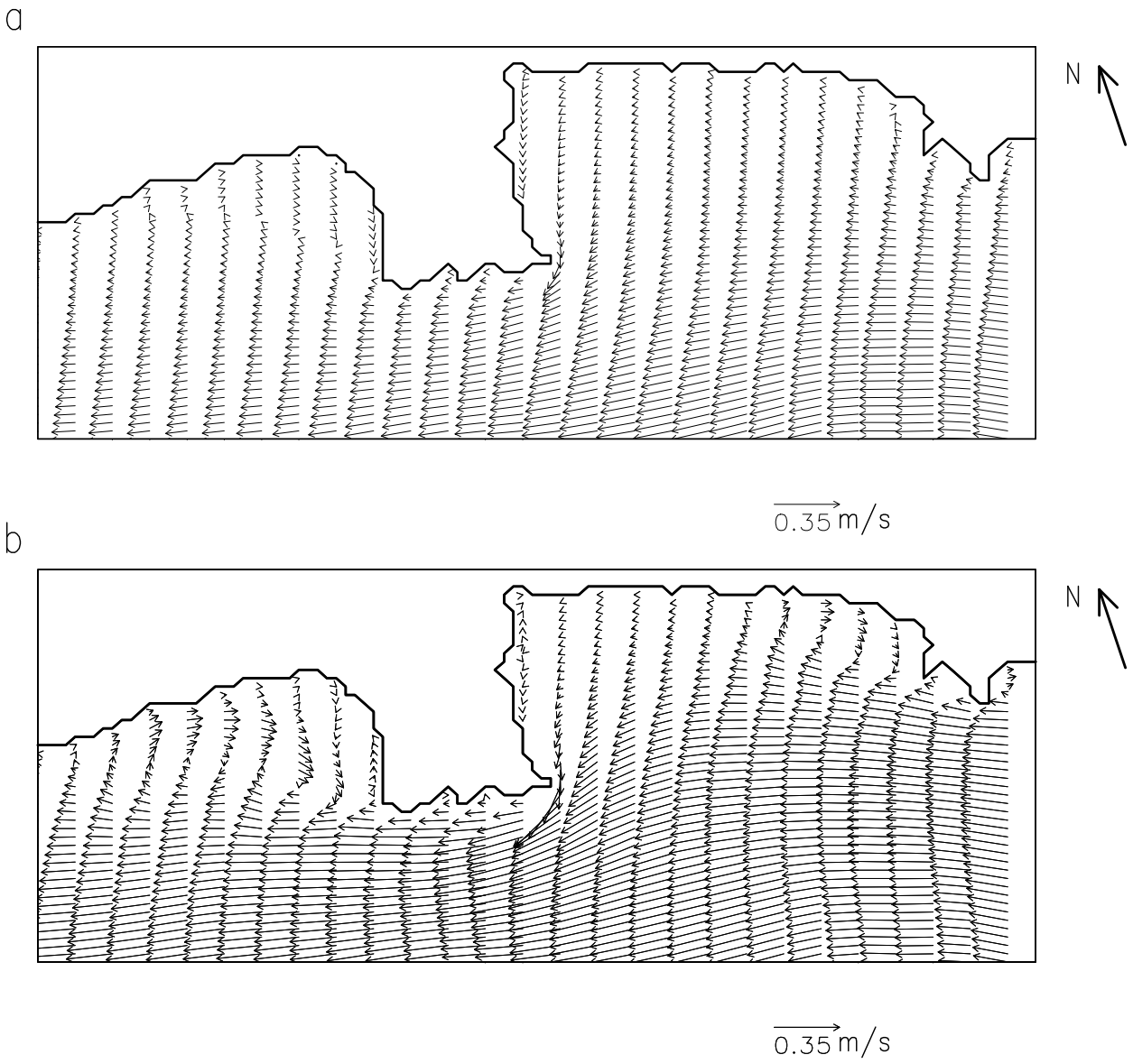

Figure 13: Experiment 'realistic bathymetry'. Depth-average velocity vectors; a) 2D case; b) 3D case.